Simulation of Continuously Variable Transmission Chain Drives with Involute Inter-element Contact Surfaces

by

THOMAS HEENAN BRADLEY
B.S. (University of California, Davis) 2000

THESIS

Submitted in partial satisfaction of the requirements for the degree of

MASTER OF SCIENCE

in

Mechanical Engineering

in the

OFFICE OF GRADUATE STUDIES

of the

UNIVERSITY OF CALIFORNIA

DAVIS

Approved:

_____

_____

_____

Committee in Charge

2003

ABSTRACT

Static and dynamic simulations of a continuously variable transmission (CVT) chain and pulley system are developed in the MATLAB environment to determine the effect of a power transmissions chain with involute inter-element contact surfaces on polygonal action in CVT systems. The static simulations consist of a geometric model of the kinematics of the CVT chain and are used as a design tool for investigating tradeoffs in contact surface design. The dynamic simulations consists of a system of lumped parameter rigid body models that represent the elements of the CVT chain and the pulleys of the CVT. The chain elements are joined using compliance and damping elements. The chain system interacts with the pulleys through Hertzian contact compliances and a two-dimensional explicit slip-stick friction model. The characteristics of the chain and pulley system are chosen to emulate a prototype 2L CVT chain manufactured by Gear Chain Industrial. The simulated static and dynamic behavior of this CVT chain exhibits reduced polygonal action when compared to a CVT chain with pinned-joint inter-element contacts.

ACKNOWLEDGEMENTS

This research has been supported in part by the United States Department of Energy Graduate Automotive Engineering Education Fellowship, Koyo Seiko Corporation Ltd. and Gear Chain Industrial B. V. Of course, this project would have been impossible without the support of Dr. Andy Frank and the students and staff of the University of California, Davis Hybrid Electric Vehicle Research Center. I have been privileged to work among this group of talented and dedicated individuals.

TABLE OF CONTENTS

LIST OF FIGURES

LIST OF TABLES

LIST OF SYMBOLS

Symbol	Description	Units
a	Diameter of contact patch	[m]
A	Area of load bearing material in chain link	[m^2]
A_b	Position of the upstream inter-element contact when chain is uncurved in the chain element reference frame	[m]
A_bc	Position of the upstream pin to pulley contact when chain is uncurved in the chain element reference frame	[m]
β	Pulley half-angle	[rad]
B_b	Position of the downstream inter-element contact when chain is uncurved in the chain element reference frame	[m]
d	Static mid-span peak to peak displacement in the y_e direction	[m/s]
δ	Contact displacement perpendicular to contact surface	[m]
dh	Distance in the y_e direction between the point tangent to contact circle and parallel to chain span and the point of pin to pulley impact	[m]
DV	Karnopp friction stick velocity	[m/s]
ε	Angular difference between θ and angle between x_b and x_e for chain elements in pulley contact	[rad/sec]
E, E^*	Young's modulus	[Pa]
F	General contact force	[N]
F_{comp}	Compressive pin to pulley contact force	[N]
F_{damp}	Compressive pin to pulley damping force under contact	[N]
γ	Angular difference between θ_i *and* θ_{i+1} for chain elements in pulley contact	[rad/sec]
g	Acceleration due to gravity	[m/s^2]
h	Vector of inter element contact forces for dynamic chain system	[N]
i	Index of chain elements	[-]
I_link	Inertia of chain element about its center of gravity	[kg m^2]
k_lin	Translational stiffness of inter-element joint for validation	[N/m]
k_rot	Rotational stiffness of inter-element joint for validation	[N/rad]
$k_{elastic}$	Elastic pin stiffness in compression	[N/m]
k_{hertz}	Herztian contact stiffness	[N/m]
$k_{pin\_bending}$	Linear stiffness of pin to bending forces	[N/m]

κ_s	Herztian contact stiffness	[N/m]
K_{spring}	Translational stiffness of inter-element joint for validation	[N/m]
L	Approximate length of chain link	[m]
l	Chain span length	[m]
L	Pin length in *z_e* direction	[m]
λ	Vector of contact forces for dynamic chain system	[N]
M	Mass of chain element	[kg]
μ_d	Dynamic coefficient of friction	[-]
μ_s	Static coefficient of friction	[-]
n	Mode number	[-]
n_{plates}	Number of link plates per chain element	[-]
P	Contact force	[N]
P	Chain element momentum	[kg m/s]
θ	Angle from *y_e* axis for chain pin in contact with the pulley	[rad]
q	State vector for dynamic chain system	[-]
Q_i	Position vector for point of pin to pulley contact	[m]
θ_t	Angular difference between element and earth coordinate systems	[rad]
R	Radius on the pulley of the equilibrium contact circle	[m]
R	Radius of cylindrical body under contact	[m]
ρ	1-dimensional density of chain span	[N/m]
Rb	Involute base radius	[m]
$S1$	Linear distance traveled by the chain span after contact with pulleys	[m]
T_t	Coordinate transformation matrix from earth to chain element body coordinates	[-]
τ	Natural period of oscillation of single chain element	[s]
t_c	Period of Hertzian contact	[s]
T_{cont}	Analytically derived natural period of oscillation for continuous chain span	[s]
T_{num}	Numerically derived natural period of oscillation for discrete chain span	[s]
T_{tens}	Tensile force in chain span	[N]
υ	Poisson's ratio	[-]
v	Chain span linear velocity	[m/s]
v,V	Chain span and chain element velocity	[m/s]
V_{pul}	Relative velocity of the pulley to the chain element for	[m/s]

	validation	
ω	Rotational Speed of the pulley (counter-clockwise +)	[rad/sec]
x_b	Unit vector in the chain element reference frame	[-]
x_e	Unit vector in the earth reference frame	[-]
x_i	Displacement along the involute contact surface in the *x_b* direction	[m]
x_{output}	Vector of equilibrium states for static simulation	[-]
y_b	Unit vector in the chain element reference frame	[-]
y_e	Unit vector in the earth reference frame	[-]
y_i	Displacement along the involute contact surface in the *y_b* direction	[m]
z_e	Unit vector in the earth reference frame	[-]

INTRODUCTION

Continuously Variable Transmission Drive Technologies

In automotive applications, continuously variable transmissions (CVTs) are proven to give significant improvement in vehicle fuel economy over conventional automatic transmissions because of the higher ratio range, lower speed torque converter lock-up, and continuously variable engine operation control available in a CVT [Hirano 1991; Hendricks 1993; Kluger 1999]. Presently, most automotive CVTs brought to production have been of the Reeves type shown in Figure 1, utilizing movable cone pulleys and a torque transmitting belt or chain [Reeves 1897]. A vast majority of automotive CVTs have incorporated a Van Doorne CVT push-belt, shown in Figure 2, because it is an available and proven technology. Automotive application of CVTs, in general, are limited to compact vehicles because of the low torque capacity and low power transmission efficiency of Van Doorne CVTs [Brandsma 1999; Abo 2000; Ide 2000].

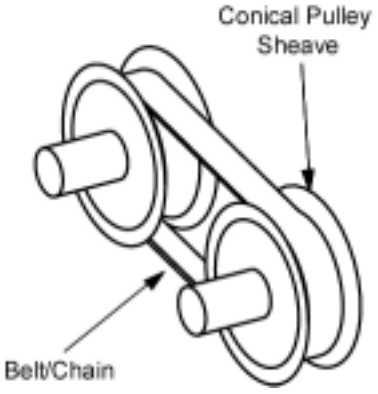

Figure 1. Reeves-type Continuously Variable Transmission

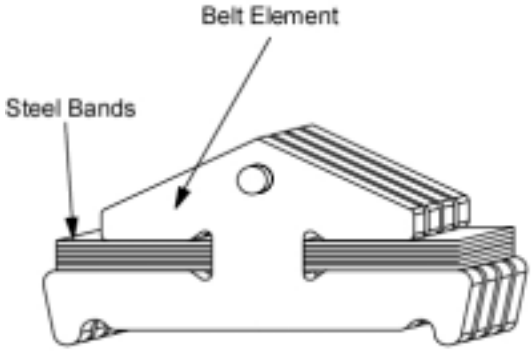

Figure 2. Van Doorne CVT Belt Assembly

Various technologies have been developed that improve on the torque capacity and power transmission efficiency of the Van Doorne CVT to allow application of CVT technology to full-sized vehicles. These technologies include toroidal CVTs, hybrid (aluminum/composite) belt CVTs, and CVT chains [Takahashi 1999; Tanaka 1999; van Rooij 2002]. CVT chains are perhaps the most promising of these technologies because of their very high torque capacity, high efficiency and low-cost materials and manufacturing processes [van Rooij 1991]. Chain CVT as manufactured by LuK, Borg Warner and others are usually characterized by increased noise and vibration emissions compared with Van Doorne CVTs because of the discrete nature of the chain drive [Avramidis 1986; van Rooij 1993; Bradley 2002]. To address these problems, Gear Chain Industrial B.V. (GCI) has developed a CVT chain that uses involute inter-element contact surfaces to minimize noise and vibration.

GCI CVT Chain Design Description

The GCI CVT chain is made up of three types of element: links (1), pins (2) and strips (3). Figure 3 is an illustration of these parts assembled into an interlocking chain.

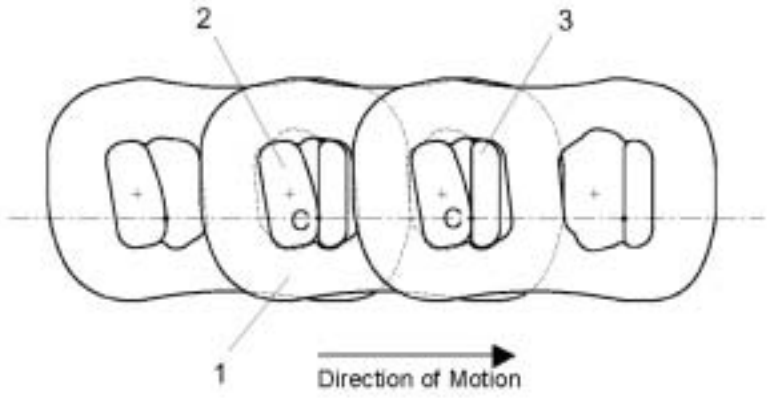

Figure 3. GCI Chain Assembly [van Rooij 1996]

When assembled, the pins are fixed to the leading link and the strips are fixed to the following link, where the leading link is in the direction of motion. The GCI chain can use the same conical pulleys that are used for the Van Doorne belt, allowing direct replacement. Torque is transferred in the CVT by traction between the CVT pulleys and the pins of the chain. Because the pins are wider than the strips, only the pins contact the pulley surface and only the pins are subjected to compressive loading from the pulleys. Unlike the Van Doorne CVT belt, torque is transmitted by tension in the chain. The tension in the chain causes a line of contact between the pins and the strips of each element at point C.

Polygonal Action

Polygonal action is a phenomenon that is unique to the dynamics of chain drives, including CVT chains. Polygonal action is a chain span vibration caused by the effect of discrete links entering the pulley. When a continuous chain enters the pulley at the equilibrium radius, the velocity of the link is tangential to the circle defined by the equilibrium radius. When a discrete chain enters the pulley there is a component of the velocity of the link that is perpendicular to the pulley surface.

The discritization of the chain into chain elements has two effects that are the cause of the mid-span vibration called polygonal action. The first effect is a dynamic effect caused by impact of the chain link against the pulley. This impact can excite vibrations in the chain span because of rapid acceleration of the impacting link. The second effect is a semi-static effect caused by movement of the links that are in contact with the pulley along an arc dictated by the pulley movement. As the link moves around the pulley from the point of entrance, the motion of the link has a vertical component as

the pin is carried around the pulley. This has the effect of inducing chain span vibrations of amplitude *d* as the entering pin moves the chain span behind it. These two types of polygonal action are illustrated in Figure 4.

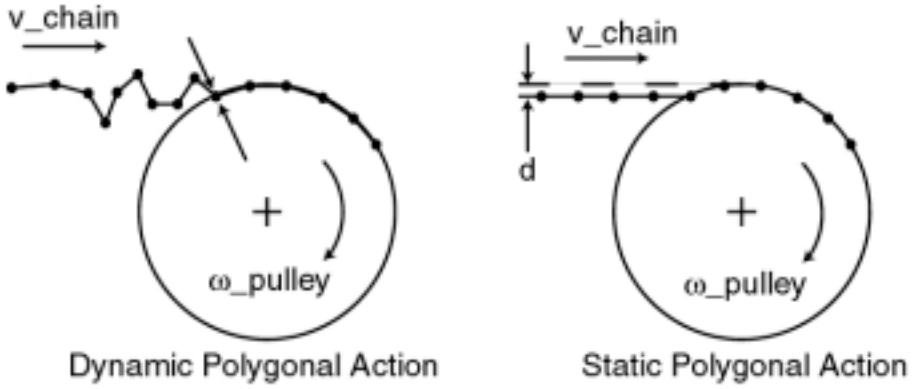

Figure 4. Illustration of Polygonal Action

The effect of polygonal action on the efficiency, noise output and vibration of the chain is greater as the chain pitch increases and the pulley diameter decreases [Avramidis 1986]. This has special implications for CVTs because the pulley diameter can vary continuously. Various schemes have been devised to eliminate polygonal action in CVT chains including multiple pitch chains [Avramidis 1986], dynamic chain tensioners [Wagner 2001], and asymmetrical link configurations [Sedlmayr 2002].

The GCI CVT chain is designed to minimize the vibrations and losses that are caused by polygonal action by incorporating involute inter-element contact surfaces. In the GCI CVT chain the pin is shaped like a circle involute and the strip is a flat plane against which the pin makes contact. When the pin enters the CVT pulley, rotation of the upstream link causes the contact point between the link in question and the upstream link to move along the curved face of the pin. The movement of the contact point between the pin and the strip imparts a moment to the downstream link, forcing the next pin to enter

the CVT pulley with a more tangential path. This moment is caused by the misalignment of inter-element contact forces, labeled F in Figure 5.

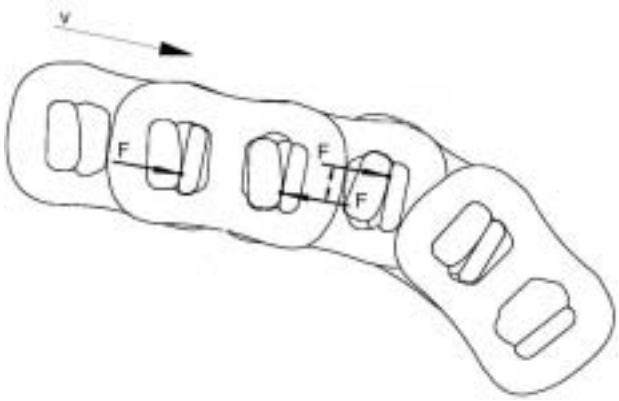

Figure 5. GCI Chain at Pulley Entrance [van Rooij 1996]

Involute contact surface CVT chains, like the GCI chain, minimize vibration and dynamic loads by forcing the chain span into a configuration where the forces at pulley contact are decreased. Although this effect is the basis of the design of the GCI chain, the behavior of involute contact CVT chains is not well understood. Optimization of the chain design has been limited by simulation tools, and the dynamic behavior of the involute contact chain is unknown. Further research into the kinematic and dynamic properties of the involute contact CVT chain is warranted in the interest of design optimization and a more fundamental understanding of the dynamic behavior of the chain as a component in the variator system.

Objectives

The global objective of this thesis is to analyze the kinematics and dynamics of polygonal action in involute CVT chains. Analysis is derived from two models of the motion of the CVT chain. These two models, a static/geometric model and a multibody

dynamic model are developed to simulate the behavior of the mechanical CVT chain and pulley system.

The static model serves to illustrate the concepts for design of involute CVT chains including:

- Derivation of the theory and general design configuration for the involute CVT chain
- Quantification of the tradeoffs in contact surface design and further optimization of contact surface geometry
- Comparison of the static behavior of involute CVT chains with pinned-joint CVT chains

The dynamic model is used to investigate the efficacy of the involute chain design including:

- Analysis of the dynamics of the CVT system interactions
- Use as a design tool for validation of CVT chain design theories
- Comparison of the dynamic behavior of involute CVT chains with pinned-joint CVT chains.

STATIC MODELS OF AN INVOLUTE CVT CHAIN

Design of the rolling contact surface between the pin and the strip determines the dynamic position of the links in the chain span. A series of static analyses can be used to derive the shape of the inter-link contact surface and to analyze polygonal vibration in CVT chains. These analyses are performed using two static models of the chain in the pulley entrance region.

Continuous Static Chain Model

A first static model is used to derive an optimum shape for the inter-element contact surface of the CVT chain. This model represents the chain span as a single rigid body with the assumptions that:

- The axes of all of the chain elements in the chain span are parallel to each other and to the line of action.
- The chain is under conditions of static equilibrium
- Pulleys are rigid, constant speed and unskewed
- No exit effects are transmitted from the upstream side of the chain span.

These assumptions represent a simplification of the chain geometry and thereby limit the application of its results. Despite that, the results of the continuous chain model will be used to illustrate the concept and function of the involute contact surface CVT chain.

Involute Contact Surface Derivation

To assure a minimization of polygonal action, the chain configuration must satisfy the Law of Conjugate Action. That is, the chain links must enter the pulley with a velocity tangent to the contact circle and with a linear velocity equal to the linear velocity

of the links already in contact with the pulley. A diagram of the configuration of a general CVT chain at entrance is shown in Figure 6.

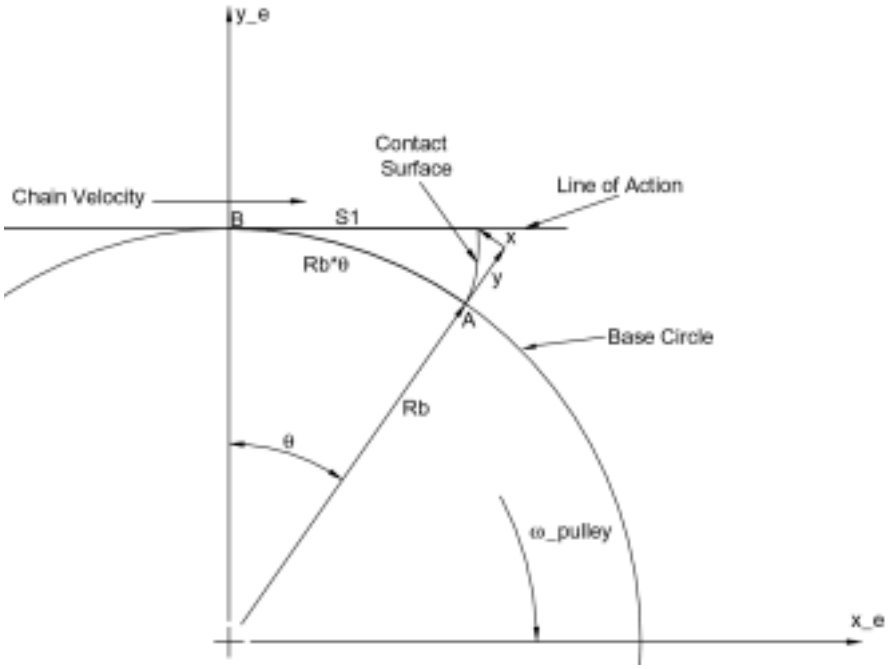

Figure 6. CVT Chain Entrance Definitions

The generic contact surface for a link is described by the vectors x and y. Colinearity along the Line of Action of the inter-element contact points is enforced by equating the *y_e* position of the contact point at position B to the *y_e* position of the contact point at position A.

$$Rb = Rb\cos\theta + y\cos\theta + x\sin\theta$$

Contant linear velocity of the chain throughout the contact sequence is enforced by equating the linear distance travelled by the chain span (*S1*) to the linear distance travelled by the link that is engaged with the pulley ($Rb\,\theta$).

$$Rb\,\theta = Rb\sin(\theta) + y\sin(\theta) - x\cos(\theta)$$

Solving for $x(\theta)$ and $y(\theta)$ gives the equation of the pin contact surface that satisfies the Law of Conjugate Action. The solutions are the equations of the involute of circle of radius, *Rb* [Khiralla 1976]:

$$x = Rb\left[\sin(\theta) - \theta\cos(\theta)\right]$$

$$y = Rb\left[\cos(\theta) + \theta\sin(\theta)\right].$$

Under the assumptions of this analysis, giving the inter-element contact surface the shape of this involute satisfies the Law of Conjugate Action minimizes polygonal action at a single radius. Again, this analysis assumes a simplified motion of the chain span but is valid as an illustration of the theory and general design configuration for the involute CVT chain

Limitations of the Continuous Static Chain Model

The contact surface involute can only be optimized for one radius and therefore only one ratio. The value assigned to *Rb* defines the radius at which the equilibrium line of action is tangent to the pulley contact circle, where polygonal action is minimized. This condition is illustrated in Figure 7. As the equilibrium radius of the chain increases with changing ratio, the positions of the Line of Action and the line tangent to the chain contact circle diverge. This effect forces the chain to enter the pulley at a radius not equal to the radius of the equilibrium contact circle. An accurate description of this effect is necessary to choose a value of *Rb* that minimizes polygonal action over a wide span of ratios.

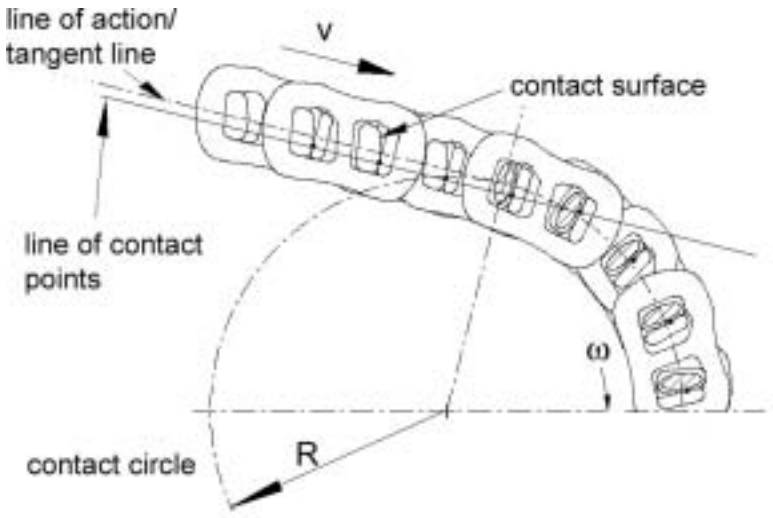

Figure 7. Involute Chain, Line of Action Tangent to Contact Circle [van Rooij 1996]

The goal of the design of the involute contact CVT chain is to transmit entrance effects upstream to lessen the impact of the pin to the CVT pulley. Understanding these entrance effects demands a second, more detailed geometric model of the chain span.

Discrete Static Chain Model

The objective of the Discrete Static Chain Model is to address the limitations of the Continuous Static Chain Model, to analyze the tradeoffs in contact surface design and to compare the behavior of the involute CVT chains with pinned-joint CVT chains. In order to expand the validity of the static chain CVT model to encompass these subjects, the model will be expanded to represent five chain elements in the entrance zone of the pulley. Modeling assumptions are as follows:

- As before, static conditions, rigid elements and pulleys, and no exit effects transmitted from the upstream side of the chain span.
- Now, the position and rotation of the five elements are defined by three independent coordinates (x, y, θ).

- The angular position of the 6th link upstream of the analysis is assumed to be tangential to the contact circle, $(\theta_i) = 0$.
- The chain does not creep or slip while in contact with the pulleys.
- All pin to pulley contact occurs at the equilibrium radius.

Formulation of Equations

For this analysis, new definitions for the intra-element geometry of the chain are required. The location of the link contact surfaces are described using the vectors shown in Figure 8. **A_b** and **B_b** describe the location of the contact points for the link in a straight chain span using body coordinates. The vector $\begin{bmatrix} x \\ y \end{bmatrix}$ describes the shape of the involute from the end of **A_b** and **B_b**, and is also in body coordinates.

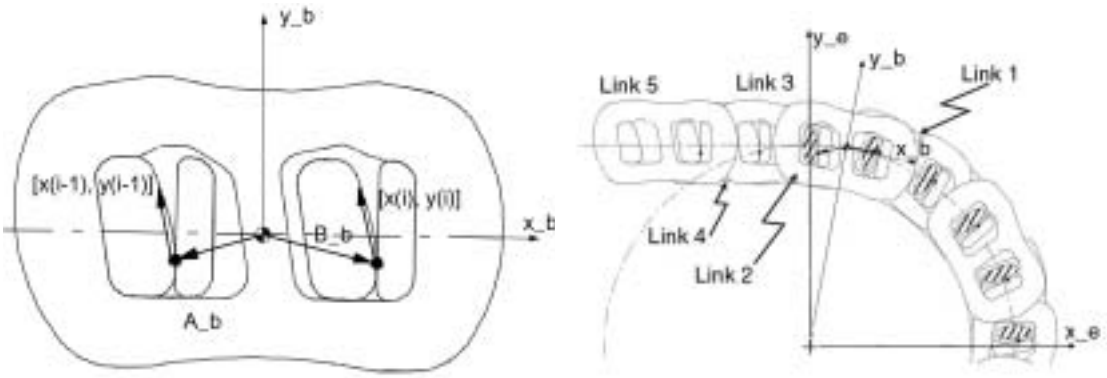

Figure 8. Chain Element Vector and Coordinate Definitions (as in [van Rooij 1996])

The geometry of the CVT chain system is described using two equations per chain element contact.

Equation (1) dictates that the inter-element contact points are colocated, that the position of the upstream contact point in the *y_e* direction for link *i* is equal to the *y_e* position of the upstream contact point for link *i*+1:

$$\begin{bmatrix}0 & 1\end{bmatrix}\cdot\left\{\mathrm{Q_i}+T_i\cdot\left(-A\_bc+A\_b+\begin{bmatrix}x_i\\ y_i\end{bmatrix}\right)\right\}= \\ \begin{bmatrix}0 & 1\end{bmatrix}\cdot\left\{\mathrm{Q_{i+1}}+T_{\mathrm{i+1}}\cdot\left(-A\_bc+A\_b+\begin{bmatrix}x_{\mathrm{i+1}}\\ y_{\mathrm{i+1}}\end{bmatrix}\right)\right\} \tag{1}$$

where the coordinate transformation matrix from link body coordinates $\begin{bmatrix}x\_b\\ y\_b\end{bmatrix}_i$ to global coordinates $\begin{bmatrix}x\_e\\ y\_e\end{bmatrix}_i$ is $T_i=\begin{bmatrix}\cos(\theta_i) & -\sin(\theta_i)\\ \sin(\theta_i) & \cos(\theta_i)\end{bmatrix}$.

(2 relates the positions of the contact points Q1 and Q2 to one another in both the *x_e* and *y_e* directions, assuring that the chain element contact surfaces are contiguous:

$$Q_2+T_2\cdot\left(-A\_bc+B\_b+\begin{bmatrix}0\\ \frac{1}{2}Rb(\Delta\theta_r)\end{bmatrix}\right)= \\ Q_1+T_1\cdot\left(-A\_bc+A\_b+\begin{bmatrix}x_1\\ y_1\end{bmatrix}\right) \tag{2}$$

where $\frac{1}{2}Rb(\Delta\theta_r)$ is the arc length measured out by the involute at an angle of $\Delta\theta_r$.

Applying these same relations to each element in the system of six links (five of which are not in contact with the pulley) along with some initialization equations allows for the generation of a system of 16 simultaneous non-linear algebraic equations. The coordinate vector solution (x_{output}) corresponds to a state of static equilibrium of the chain system.

$$x_{output}=\left[\left(Q_{3-6}\right)^T \quad \theta_{1-6} \quad \gamma \quad \varepsilon\right].$$

Solver

These 16 simultaneous equations are solved using a least squares iteration routine named *fsolve,* part of the MATLAB Optimization Toolbox. The equilibrium

configuration for the chain span is calculated at discrete points encompassing the movement of one element length. Derivative discontinuity in the results of the static CVT chain model is present due to the very small values being examined, and the iterative nature of these solutions. A copy of the program used to perform these calculations is presented in Appendix 1.

Results

Figure 9 shows the general configuration of the CVT chain at entrance as calculated using the Discrete Static Chain Model. In this figure, the motions of the chain elements are from left to right and the rotation of the pulley is clockwise. The chain is in permanent contact with the pulley after contacting the pulley at the labeled points. The geometry of the involute contact chain simulates the geometry of the GCI CVT chain. For comparison, the path of a chain with pinned inter-element contacts is also illustrated. The pinned contact chain configuration represents a chain with a pin connection between chain elements, similar to the chain shown in Figure 10. Both configurations are modeled with equal pitch.

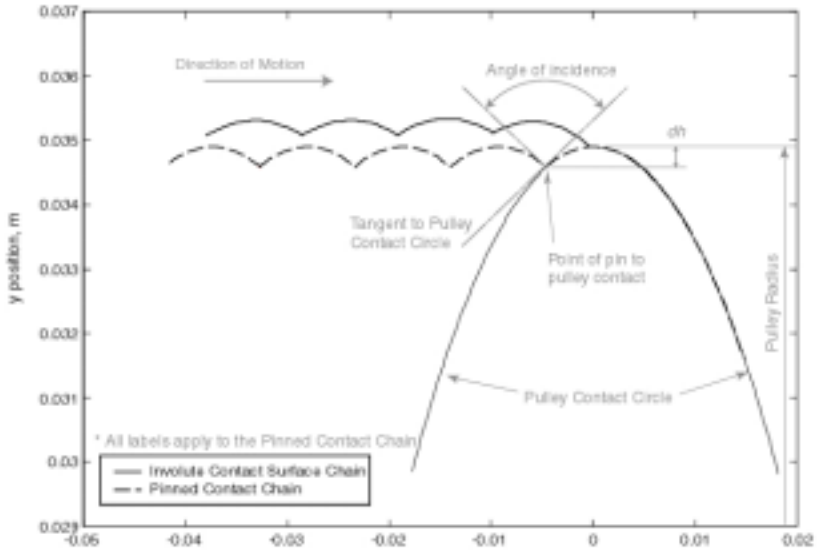

Figure 9. Chain Path and Definitions for Involute and Pinned CVT Chains (Vertical axis is exaggerated for clarity)

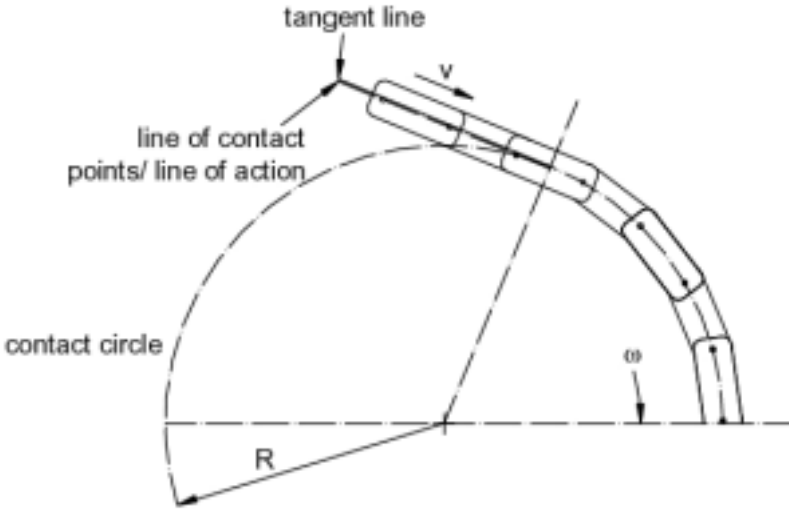

Figure 10. Pinned Joint CVT Chain, Line of Action Displaced from Tangent Line

Initially, the results of this simulation will rely on two geometric quantities from the static chain configuration to predict the type and degree of polygonal action. The quantity *dh*, defined in Figure 9, is related to the occurrence of the semi-static type of polygonal action. The angle of incidence, also defined in Figure 9, is related to the force experienced by the chain element at impact to the pulley, and therefore is an indicator of the dynamic type of polygonal action. Both *dh* and the angle of incidence will be determined from calculation of the equilibrium configuration of the CVT chain in order to characterize the type and magnitude of polygonal action present in each chain design.

CHARACTERIZATION OF SEMI-STATIC POLYGONAL ACTION - As can be seen in Figure 9, the position and configuration of the involute contact surface chain are very different from the position and configuration of the pinned contact chain. Each line represents the path in space of the pin-to-pulley contact point. For the involute contact chain, the impact of the chain pin with the pulley occurs at a *y*-position of 34.9 mm, ie. *dh* is equal to 0. For the pinned contact chain, the pin-to-pulley contact occurs at a *y_e*

position of 34.6 mm, ie. *dh* = 0.3 mm. Because *dh* has been chosen as an indicator of semi-static polygonal action, this simulation indicates that the involute contact chain should exhibit less semi-static polygonal action than the pinned contact chain at a contact radius of 34.9 mm.

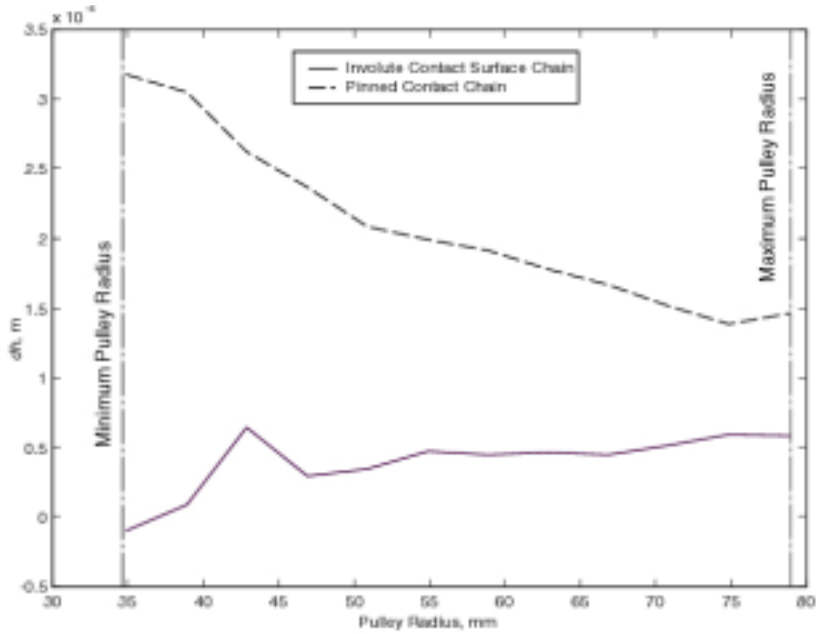

Figure 11. Y-direction Distance of Impact from Tangent for Involute and Roller CVT Chains

Figure 11 shows the relationship between the equilibrium radius of the chain and the distance of the point of impact from tangent, *dh*. Although *dh* for the involute chain does increase slightly with increasing pulley radius, at all radii *dh* for the involute chain is smaller than *dh* for the pinned contact chain. This suggests that the involute contact chain will exhibit less semi-static polygonal action than the pinned contact chain at all radii.

CHARACTERIZATION OF DYNAMIC POLYGONAL ACTION - Figure 12 shows the relationship between the equilibrium radius of the CVT chain and the angle of incidence of the chain element as it comes in contact with the pulley contact circle. As should be expected, the angle of incidence decreases at higher pulley radii. Also, the angle of

incidence of the involute chain is less than the angle of incidence of the pinned contact chain. Because a greater angle of incidence demands a greater acceleration to move the chain element towards a circumferential path, this simulation suggests that the involute chain will experience less impact loading than the pinned contact chain and therefore less dynamic polygonal action, at all pulley radii.

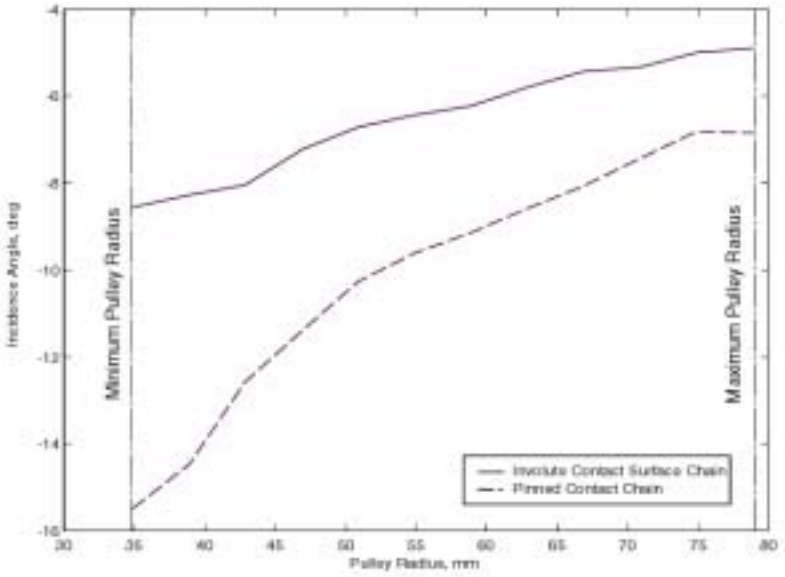

Figure 12. Impact Incidence Angle for Involute and Roller CVT Chains

Static analysis shows that involute inter-element contact surfaces have the effect of decreasing the magnitude *dh* and the angle of incidence of the chain element at contact. These two effects combined will result in decreased polygonal action, and improved vibration and efficiency characteristics for the CVT.

FURTHER OPTIMIZATION OF INVOLUTE CHAIN DESIGN - The involute contact surfaces of the GCI chain are designed to minimize *dh* at the smallest pulley radius and thereby reduce polygonal action at all radii. Other factors that may contribute to polygonal action, such as angle of incidence and amplitude of static mid-span displacement (defined as *d* in Figure 4), have not been considered in the design

optimization. This small scope of the GCI design optimization is a result of the limitations of preexisting static models of the GCI CVT chain.

The static model designed and implemented as part of this research allows for calculation of the static equilibrium configuration of the CVT chain at various configurations. This flexibility allows design optimization to include minimization of other factors that are contributors to polygonal action. This section of the results will show how the design of the involute contact chain can be improved for lower *dh*, lower angle of incidence and lower midspan vibration amplitude using the Discrete Static Chain Model described above. Although this section of the static simulation results is somewhat of an aside, it provides insight into the tradeoffs present in optimization of the involute contact surfaces.

Figure 13 shows the effect that varying the involute base radius, *Rb*, has on the location of contact of the chain to the pulley. As should be expected, the simulation shows that the pinned contact chain impacts the pulley under the line tangent to the pulley contact circle at point 1. As shown in Figure 13, the involute chain with a base radius, *Rb*, of 56 mm impacts exactly at the tangent line at position 2. By increasing the base radius of the involute, the chain configuration is changed so that the chain element contacts on the other side of the pulley at position 3. In this case, *dh* is still positive because the chain has impacted below the tangent line.

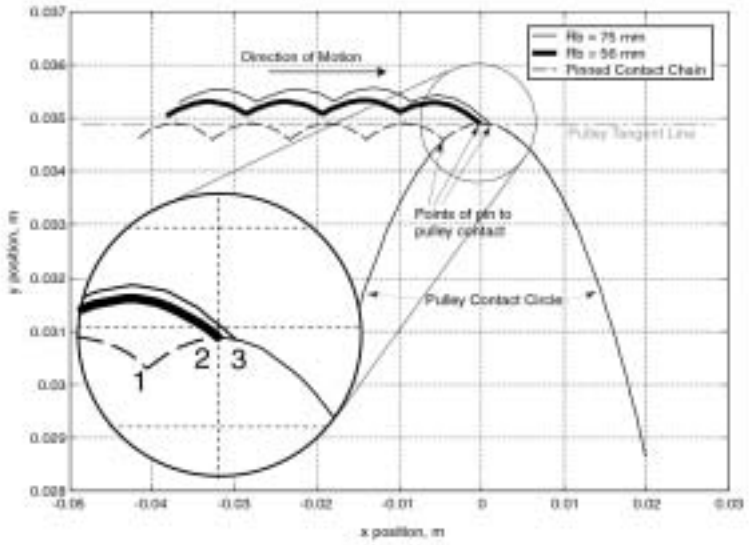

Figure 13. Chain Path for Involute Chains of Different Base Radii

By increasing *Rb* to greater than 56 mm, polygonal action can be further reduced in two ways. First, as shown in Figure 13, the angle of incidence of the pin-to-pulley impact is reduced with increasing *Rb*. Angle of incidence has earlier been equated to dynamic polygonal action. The second benefit of a configuration incorporating a larger *Rb* is not evident without an investigation of the effect of ratio on the quantity *dh* for various values of *Rb*. As shown in Figure 14, the average value of *dh* at all radii for the involute chain of *Rb* = 75mm is 62% smaller than the value for the involute chain with *Rb* = 56mm. A smaller value of *dh* means lower impact forces and less semi-static polygonal action.

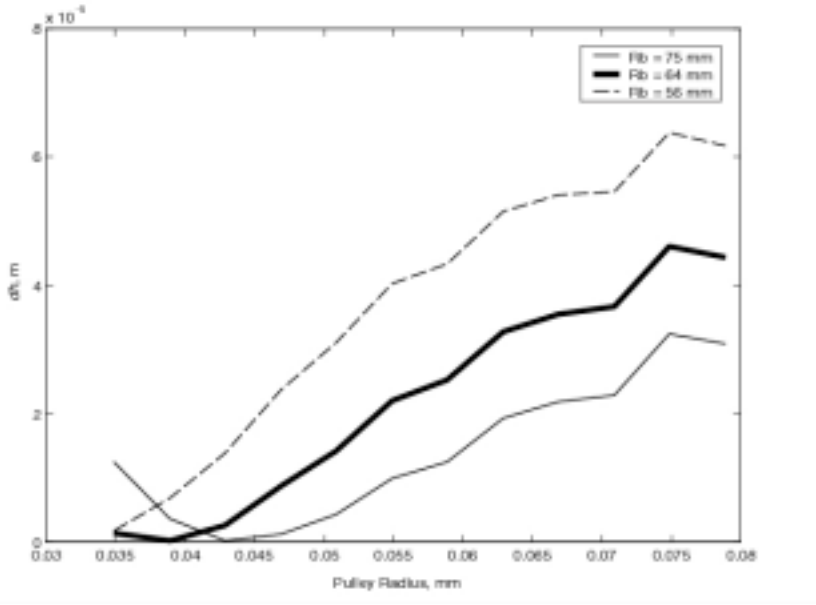

Figure 14. Y-direction Distance of Impact from Tangent for Involute Chains of Various *Rb*

As a final design configuration check, Figure 15 shows the amplitude of movement of the chain element 4 links upstream from the impacting chain element. The chain span displacement amplitude, represented analytically by the peak-to-peak vertical displacement of element no. 5, does not increase with increased values of *Rb*. This suggests that the benefits exhibited by the chain with *Rb* > 56mm do not come at the expense of chain span displacement.

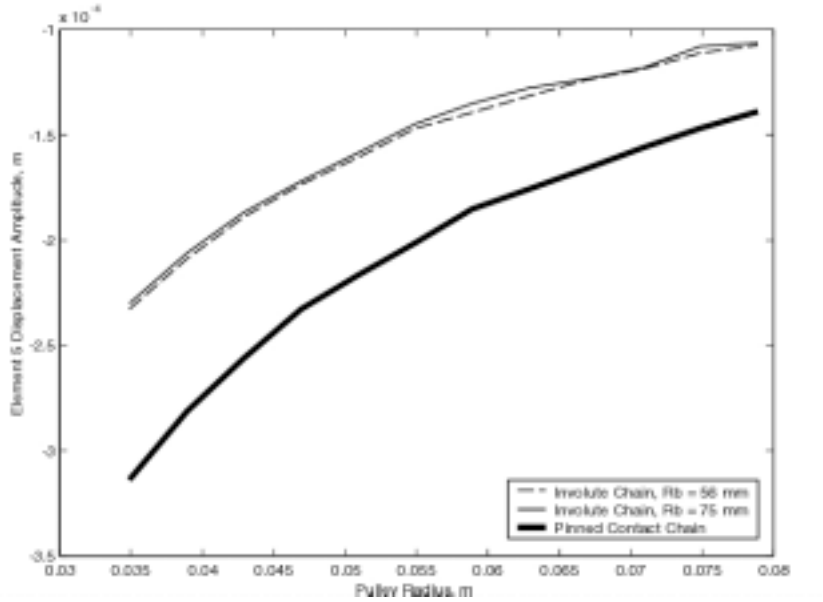

Figure 15. Amplitude of Element no. 5 Oscillation in *y_e* direction for Involute Chains of Various *Rb*

A static analysis of the equilibrium position of the chain elements shows that by increasing the base radius of the involute contact chain, the configuration parameters associated with polygonal action in the chain system (*dh*, angle of incidence, mid-span vibration amplitude) are either reduced or unaltered. This preliminary design represents a further optimization of the GCI chain configuration under static assumptions and is a result of the development of the Discrete Static CVT Chain Model as a tool for design and analysis. Validation of the design must come from further analysis and experimental testing.

STATIC MODELING CONCLUSIONS - New flexible modeling tools for further development and optimization of the chain design have been developed as part of this research. The design concept of the involute contact chain has been derived and discussed. The design tradeoffs in of the involute contact chain at various contact radii have been quantified. Based on these tradeoffs, an iteration of the involute contact chain design has been proposed for a further reduction in polygonal action.

DYNAMIC MODEL OF AN INVOLUTE CVT CHAIN

A dynamic simulation of the CVT chain will be used to determine the dynamic effectiveness of involute contact surfaces in reducing vibration and polygonal action in CVT chains, to verify the effectiveness of the design of the involute CVT chain. The dynamic chain model is designed to simulate the geometry of the 30 mm GCI CVT chain.

Constitutive Component Models

Chain Model Description and Validation

Various methods have been investigated for simulation and analysis of the motion of chain drives, but they can be divided grossly into static and dynamic analyses. Static analyses consist of determining chain to sprocket contact conditions and calculating forces and positions of chain links based on static calculations as performed above. Dynamic analyses consist of devising a chain model and solving for forces on the chain using dynamic calculations. Assumptions used in construction of the dynamic chain model determine which aspects of chain dynamics can be studied. [Ariaratnam 1987] modeled the chain span as a one-dimensional continuous compliant string to study dynamic chain stability. Others have studied chain polygonal action by modeling the chain with four-bar linkages. [Bothwell 1987], [Srnik 1997] and [Troedsson 2001] formulate dynamic equations using a multibody scheme with compliant constraints. Multibody dynamic simulations have the advantage of being able to capture polygonal action, chain inter-link dynamics, chain to pulley contact and entrance and exit effects.

CHAIN MODEL DESCRIPTION - Because the goal of this analysis is to evaluate sources of vibration from all of these sources, a multibody dynamic simulation with compliant constraints was chosen for this study. A planar rigid body is used to model

each element of the CVT chain. The element has 3 degrees of freedom corresponding to two in translation and one in rotation in the plane. The chain elements are coupled to adjacent links with compliance and damping elements that represent elasticity and damping in the inter-link bearings. These elements apply forces to the links in both the *x_b* and *y_b* directions in the plane based on the differential displacement and velocities of adjacent links. Differential rotation of the link does not produce reaction forces.

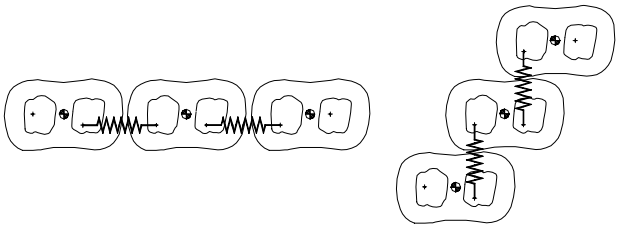

Figure 16. X and Y Direction Link Compliance Model

A multilateral contact model is used to describe the compliance between the strip of element *i* and the pin of element *i+1*. The compliance between chain elements is modeled as the series sum of compliance from Hertz contact compliance, bending of the pin and link and elastic extension of the link plates. Hertzian contact between the chain links and the pins is not considered.

HERTZ CONTACT COMPLIANCE - For the Hertz contact compliance, the strip is modeled as an elastic flat half space and the pin is modeled as an elastic cylinder. From [Johnson 1985], the contact displacement δ, of a cylinder in contact with a planar surface is:

$$\delta = P\frac{\left(1-\upsilon^2\right)}{\pi E}\left[2\ln(4R/a)-1\right] \tag{3}$$

where the semi-contact-width is

$$a = \sqrt{4PR/\pi E^*} \tag{4}$$

ELASTIC PIN BENDING - The pin is loaded by contact forces from the pulleys and by contact forces from the chain links. The position and magnitude of the loads transmitted to the pin by the links are determined by the geometry of the joint. Because the pattern of the chain links repeats every three links there are three different loading conditions for the chain pin which must be examined to derive a global or averaged compliance. The joint configuration and loading conditions for Joint 2 are shown in Figure 17. Each link-to-pin contact is represented as a point load, located at the same position as the contact point relative to the x-axis of the pin.[1]

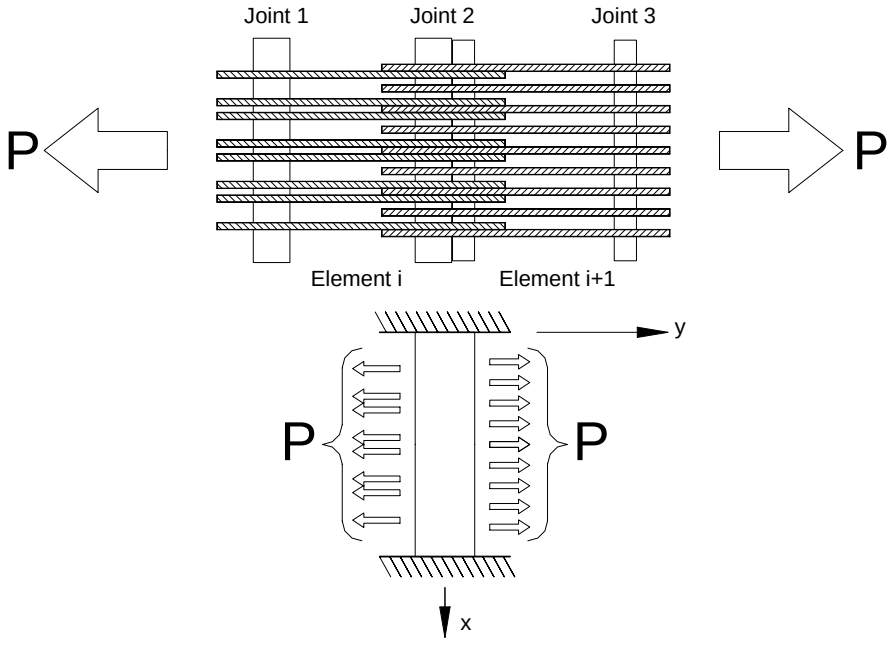

Figure 17. Element Definitions and Pin Loading Diagrams

Bending of the pin is modeled as the bending of a linear elastic, simple, slender beam under multiple point loading conditions with fully constrained ends. The

MATLAB m-file used to perform this calculation is included in Appendix 3. The deformed shape of the central axis of the chain pin is shown in Figure 18.

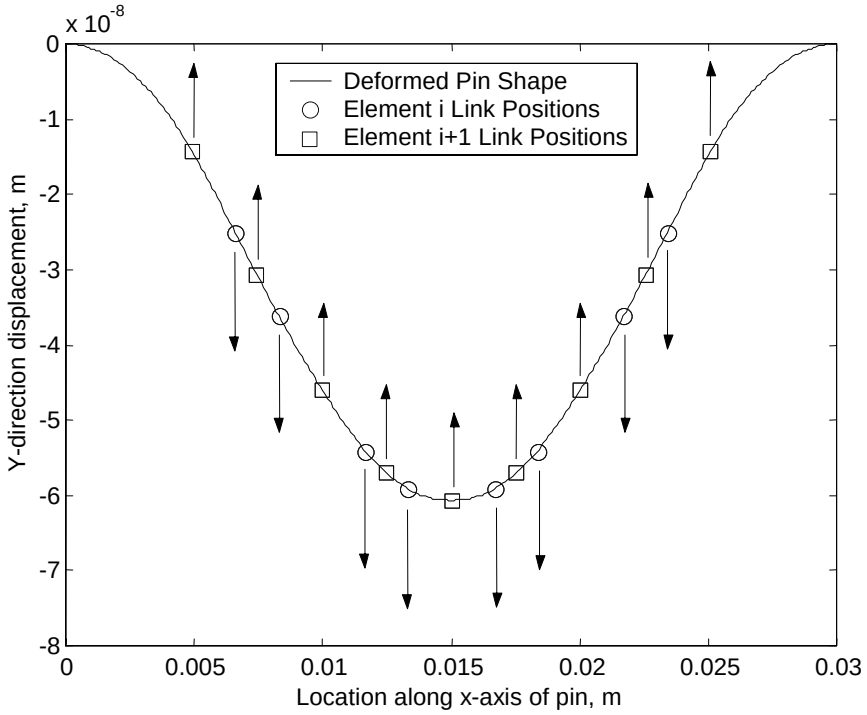

Figure 18. Pin Deformation for Joint Type 2, P = 437.5 N

The sum inter-element compliance is derived from the difference of the average link plate position for each chain element. By repeating this analysis for the three types of joints present in the GCI CVT chain an average stiffness for all chain joints can be defined as:

$$k_{pin\_bending} = \frac{3P}{\sum_{j=1}^{3}\left[\frac{\sum_{k=1}^{n_{plates}} y_{i+1}}{n_{plates}} - \frac{\sum_{k=1}^{n_{plates}} y_i}{n_{plates}}\right]} \tag{5}$$

[1] For convenience, x and y definitions used in calculation of the pin bending correspond to conventions from Mechanics of Materials. They differ from the *x_e* and *y_e* convention used in other portions of this thesis.

where *j* is the joint number, *i* is the element number, y is the displacement of the pin at each link and n_{plates} is the number of links per element.

ELASTIC LINK EXTENSION - Elastic extension of the link plates is modeled as a beam under simple tension, where $\delta = \frac{PL}{n_{plates} EA}$, and n_{plates} is the number of parallel link plates per chain element. As shown in Figure 19, the elastic extension of the link plates is more compliant than the other deformation mechanisms. All compliances are very linear over the range of applied forces encountered in the simulation, and are modeled as linear.

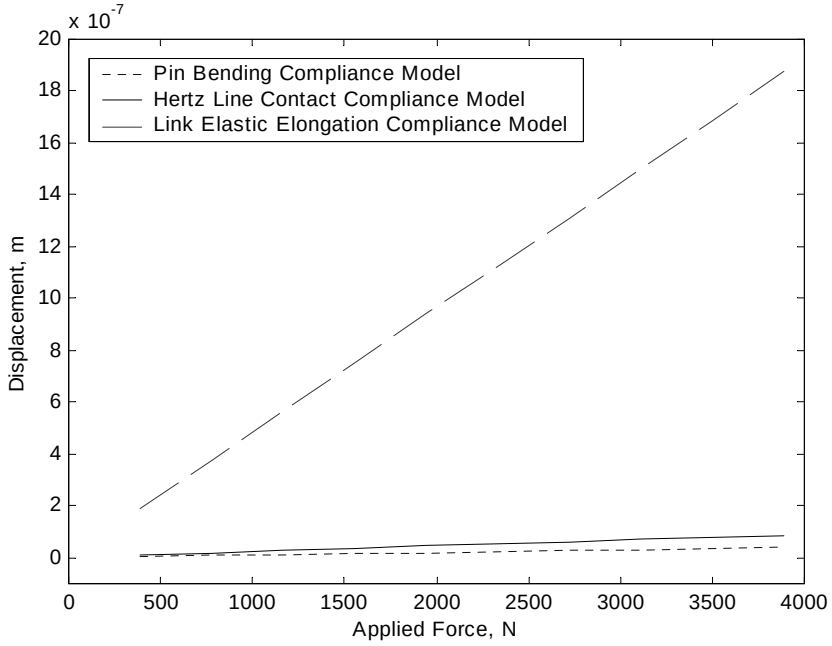

Figure 19. Modeled Sources of Inter-Element Compliance

The compliance that is derived from the series sum of these models is multilaterally applied in both the x and y-directions. The links are assembled into a chain of 75 identical elements with identical compliances.

CHAIN MODEL VALIDATION - Validation of the chain model is performed for the chain dynamics both locally at the element compliance level and at the chain span levels.

At the local, chain element level, the free response of the link will be compared to an analytical solution for a linear compliance between the links of the chain. This validation is performed by providing an initial relative displacement in the *x_e*, *y_e* and θ-directions to a link surrounded by two fully constrained, unmoving links. In this case the dynamics of the motion in each direction is decoupled by enforcing $A\_b = \begin{bmatrix} -C \\ 0 \end{bmatrix}$ and $B\_b = \begin{bmatrix} C \\ 0 \end{bmatrix}$. The undamped numerical solution of the equations of motion for a linear inter-link compliance of 3e12 N/m is presented in Figure 20.

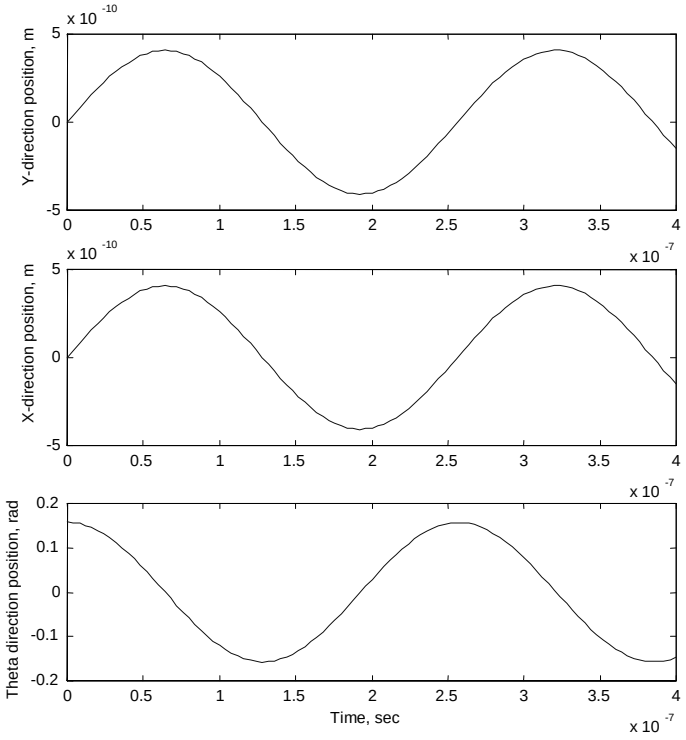

Figure 20. Chain Element Natural Period Validation

In this test case the moment of inertia of the link, *I_link*, has been chosen to make the period of rotational oscillation equal to the period of linear oscillation. The period of oscillation can be analytically calculated as

$$\tau = 2\pi\sqrt{\frac{M}{k_{lin}}} = 2\pi\sqrt{\frac{I\_link}{k_{rot}}},$$

where the rotational compliance

$$k_{rot} = r^2 k_{lin}.$$

The calculated period of oscillation is 2.56e-7 seconds, and the simulated period of oscillation is 2.56e-7 seconds. After 10 oscillations the energy of the system is conserved to within 0.3%. For a linear compliance with no damping, the equations are

proven correct and the model is considered validated at the link level against the analytical solution.

Globally, the model will be validated by comparing the numerical period of oscillation of a representative chain span to an analytical solution. Eighteen discrete elements with pinned contact surfaces are assembled into a chain between two fully constrained, immovable elements. The chain is provided an initial half period sinusoidal displacement and the equations of motion are solved using an ordinary differential equation solver. Figure 21 shows the first mode of the chain vibration for the 18 element discrete chain. The shape and period of oscillation of this mode will be validated against an analytical, continuous solution.

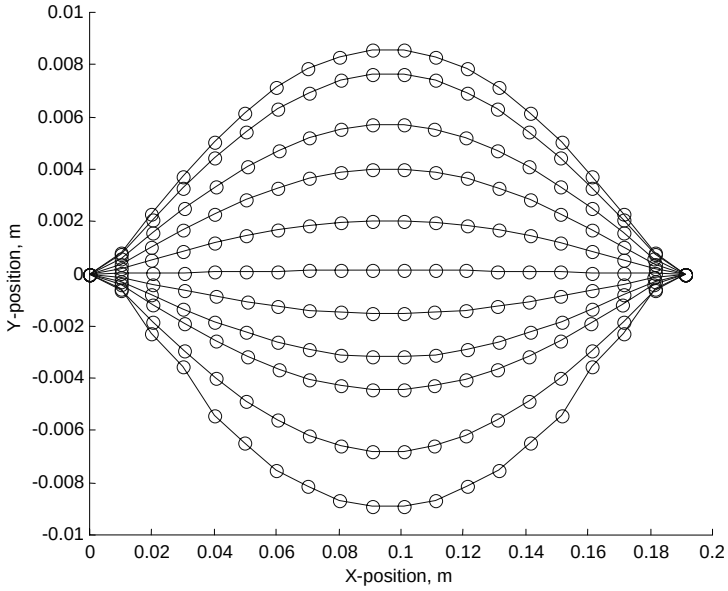

Figure 21. Chain Mode Shapes and CG Locations

By approximating the chain as a continuous heavy string under tension, the natural first order period of oscillation is defined as

$$T_{cont} = \frac{2l}{n}\sqrt{\frac{\rho}{T_{tens}}}.$$

Comparison of the numerical and analytical periods of oscillation for the chain span shows acceptable correlation considering that the analytical solution is an approximation of the behavior of the discrete chain.

Table 1. Comparison of Numerical and Analytical Span Vibration Solutions

Chain Tension T_{tens} [N]	Chain Density ρ [kg/m]	Numerical Natural Period T_{num} [sec]	Analytical Natural Period T_{cont} [sec]	Percent Difference
275	1.081	0.020	0.022	9.1%
2748	0.992	0.0067	0.0073	7.8%

The global inter-link dynamics of the chain model are considered validated against a simple analytical model.

Contact Model Description and Validation

Two fundamental tools exist for modeling of impact with friction in rigid body systems: impulse-momentum relations and compliant contact modeling [Stronge 2000]. Impulse-momentum relations are only applicable to a multi-body system where the contact compliance is either very high or very low in comparison to inter-body compliances, because this allows the assumption of simultaneous or sequential impact. Because the compliance of contact between the chain and the pulleys is of the same order as the compliance of contact between the chain links, strict impulse-momentum relations will produce erroneous results for a multibody chain simulation. Instead, a compliant contact modeling approach is required where each individual contact for each body is represented by a discrete compliance; a local contact compliance is required for both the inter-element contact and the pin to pulley contact [Stronge 2000]. The three main disadvantages of compliant contact modeling for numerical simulation of multibody contact dynamics are that it often leads to stiff differential equations, that oscillations can

occur under conditions of permanent contact and that a continuous friction law is often needed to maintain constant causality under slip-stick contact [Abadie 2000]. In the case of this simulation these problems are resolved to an acceptable degree. The nature of the differential equations are discussed in the section titled Formulation of Equations, and contact oscillations and friction laws are discussed in the section titled Contact Model Description and Validation.

CONTACT MODEL DESCRIPTION - For this simulation, a local contact compliance model is used between the pulley sheaves and the chain element. The contact compliance is modeled as the series sum of a Hertzian contact model and a linear elastic pin compliance model. A diagram of the pin to pulley contact model is shown in Figure 22. The point where the pin contact with the pulley is massless and its motion is restricted to translation in the z-direction.

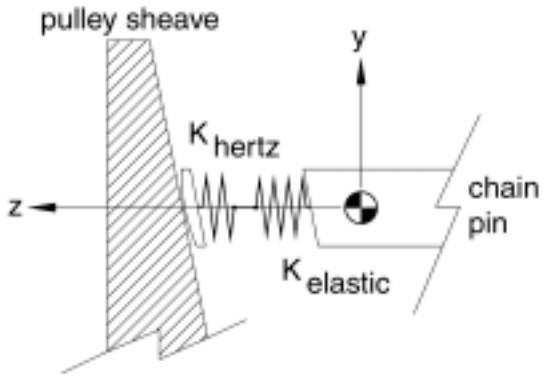

Figure 22. Pin Compliance Model

A spherical Hertzian contact model is used to represent the contact forces between the chain pins and the pulley sheaves. Although Hertzian contact relations are based on a semi-static analysis and impact mechanics are by nature dynamic, Hertzian contact relations are a widely used approximation of impact compliance [Stronge 2000] [Kraus

1997]. In the case of link to pulley contact, both the pulley sheaves and the pin contact surfaces are approximated as large radius spheres.

Sample contact laws for inelastic, spherical, Hertzian contact are:

$F_{comp} = \kappa_s \delta^{3/2}$ [Abadie 2000]

A linear-elastic model of the chain pin is used to represent the deflection of the pin under chain clamping forces. Where bending in the pin is not considered, the deflection of the pin is $\delta = \frac{F_{comp} L}{EA}$. Figure 23 shows the pin contact and elastic compliance models. The total pin compliance is the series sum of the linearized Hertzian compliance and the linear elastic compliance models.

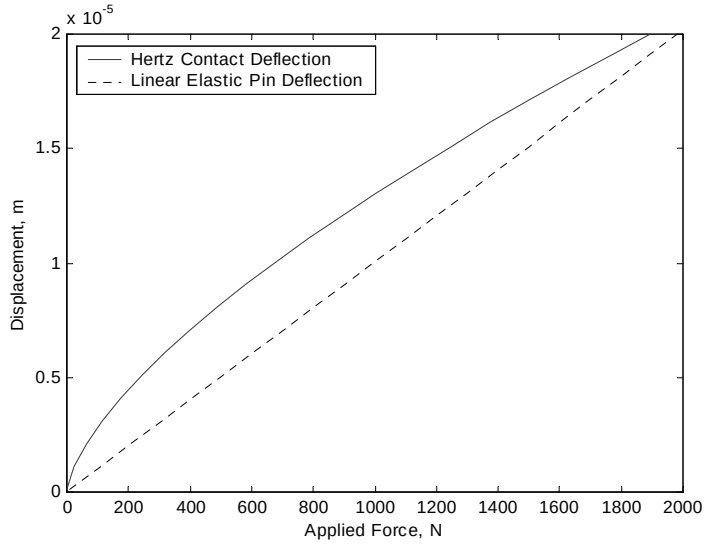

Figure 23. Chain Pin Compliance Models

CONTACT MODEL VALIDATION - The contact model is first validated for the case of an elastic impact without friction. A single chain pin is impacted against the stationary pulley model perpendicular to the surface of the pulley.

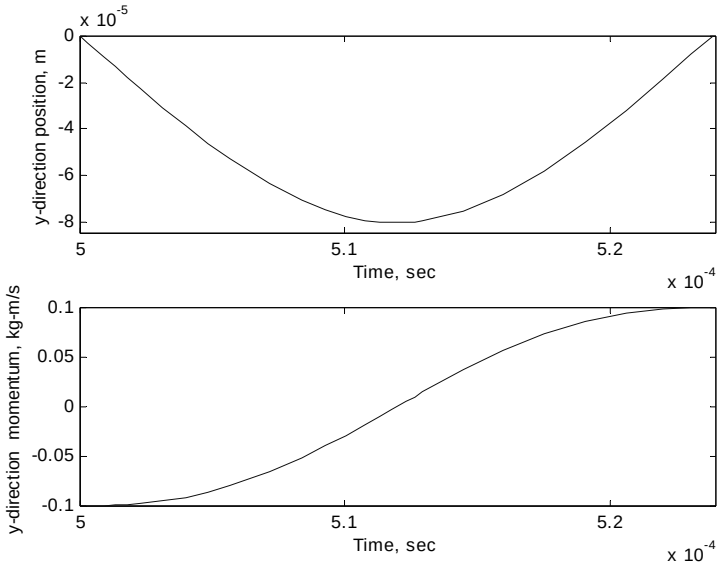

Figure 24. Frictionless Pin to Pulley Impact Simulation

The analytical solution for this problem is derived from Hertz's theory of impact. Elastic contact without friction corresponds to a Poisson or energetic coefficient of restitution of 1.0. By conservation of energy the kinetic energy of the link is equal to the potential energy at maximum displacement during impact [Stronge 2000]. Where M is the mass of the link, δ is the displacement of the impacting body, κ_s is the coefficient in Hertz's contact law, and v_0 is the initial velocity of the link, T_0, the initial kinetic energy of the system is:

$$T_0 = \frac{1}{2} M v_0^{\,2} = \int F \cdot d\delta = \int \kappa_s \delta^{3/2} \cdot d\delta \,.$$

Solving for maximum displacement:

$$\delta_{\max} = \left(\frac{5}{4} \frac{m v_0^2}{\kappa_s} \right)^{2/5} .$$

From which the maximum force is

$$F_{\max} = \kappa_s \delta_{\max}^{\,3/2} .$$

Using the method of Deresiewicz (1968), the period of contact can be obtained from

$$t_c = 2.943\left(\frac{\delta_{\max}}{v_0}\right).$$

	Simulation	Analytical Solution
Poisson Coeff. Of Restitution	0.999	1.000
Maximum Displacement (m)	8.05E-05	8.09E-05
Maximum Force (N)	1.533E+04	1.545E+04
Contact Period (sec)	2.385E-04	2.381E-04

Table 2. Contact Model Validation Results

The simulation results correspond very well to the analytical solution, and the elastic contact model is considered validated for this case.

Next, the model is validated for elastic, eccentric impact against a frictionless surface. Because the impact is eccentric the impact forces apply both a reaction force and a reaction moment to the link body. For validation of the elastic, eccentric impact model the three conditions that must be met are conservation of energy, conservation of linear momentum and conservation of angular momentum. These conditions are verified for the impact configuration corresponding to an initial angular displacement of -60 degrees. Graphical results from this test of the contact model is presented in Figure 25. Like in the chain element model only the left-hand-side of the body may make contact with the contact surface. Intrusion into the contact surface by the right-had-side of the contacting body is allowed.

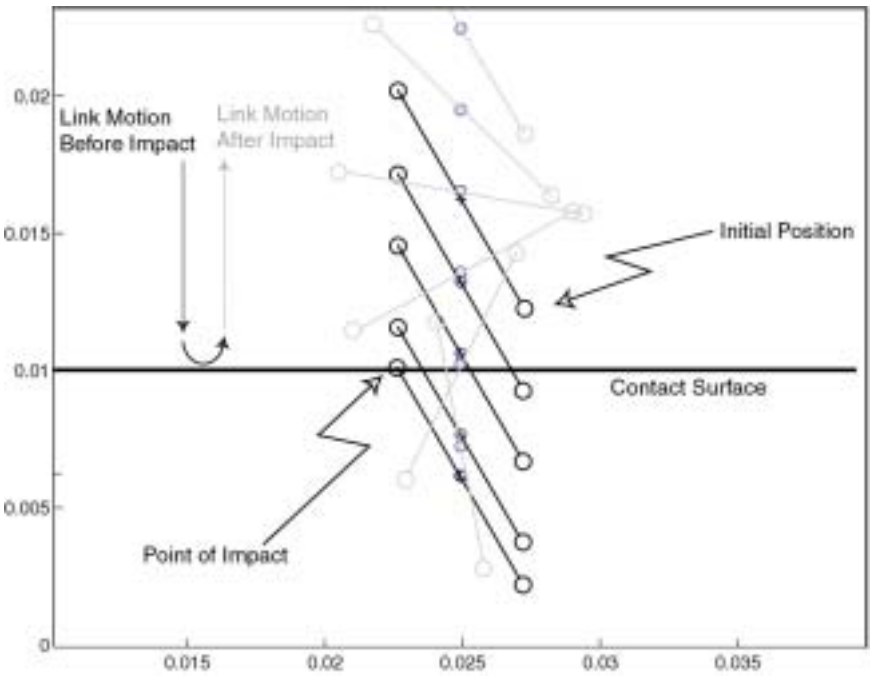

Figure 25. Frictionless Contact Model Validation

Conservation of energy is verified by calculating the Poisson coefficient of restitution. A Poisson coefficient of restitution of 1.0 represents perfect energy conservation. Conservation of linear and angular momenta are verified using the equations of motion of a rigid body acted on by an impulse *dP*. In the y-direction, $dP = M\Delta v$, and in rotation, $I\_link \cdot \ddot{\theta}_m = A\_b \times dP$. Using the results of the simulation the magnitude of the impulse *dP* can be calculated from both equations. Conservation of linear and angular momenta demands that the calculated impulses be equal.

Table 3. Rigid Body Contact Model Validation Results

Poisson Coeff. of Restitution	1.01
Y-direction Calculated *dP* (kg-m/s)	0.1610
Rotational Calculated *dP* (kg-m/s)	0.1598

As seen in Table 3, the results of the simulation obey conservation of energy and momentum. The impulse in the rotational direction is equal to the impulse in the translational direction to within 1%, and the energetic coefficient of restitution is equal to approximately 1.0. On the basis of validation under colinear and eccentric rigid body contact, the model is considered validated against the analytical solutions.

Friction Model Description and Validation

The precise characteristics of the friction interface between the links and sheaves in a chain CVT transmission are unknown. In belt CVTs, slip-stick friction is present in the contact between the belt elements and the sheaves of the transmission. Several friction models have been proposed to represent this interface in belt CVTs, including Coulombic [Gerbert 1984; Fujii 1993; Kobayashi 1998] and elastohydrodynamic friction [Micklem 1994], but it cannot lightly be presumed that the friction characteristics of a CVT chain are the same as those of a CVT belt. The contact surface in a CVT chain is, in general, characterized by lower slip rates, higher contact pressures, and higher impact forces than in CVT belts. Published experimental data for friction measurements in CVT chains are, as yet, non-existent. In constructing a simulation model of a PIV CVT chain, Srnik and Pfeiffer [Srnik 1994] use both a strict Coulomb friction model and a continuous approximation of Coulomb friction with similar results. Still, in order to improve the adaptability of the model and in an attempt to capture all dynamics of relevance, a slip-stick friction model is preferable.

FRICTION MODEL DESCRIPTION - In this simulation, a slip-stick friction model will be used that is based on the algorithm of Leine et al. [Leine 1998]. This algorithm avoids the physical and numerical problems that are associated with strict Coulomb

friction models and their continuous approximations. The equations of state produced with this algorithm are non-stiff, ordinary differential equations with constant causality.

The Leine algorithm is based on the friction model introduced by Karnopp [Karnopp 1985]. Karnopp friction defines a small band of relative velocity centered at zero with width of twice *DV*. Outside of this velocity band, the system is assumed to slip. Inside of this band, if the applied force on the system is less than breakaway friction force, the system will stick. If the force on the system is greater than the breakaway friction force, the system will transition to slip. With Karnopp friction, the system carries a small velocity error when stuck. Under stick, the algorithm of Leine et. al. forces the velocity of the system to zero to avoid the error and numerical instability associated with Karnopp friction.

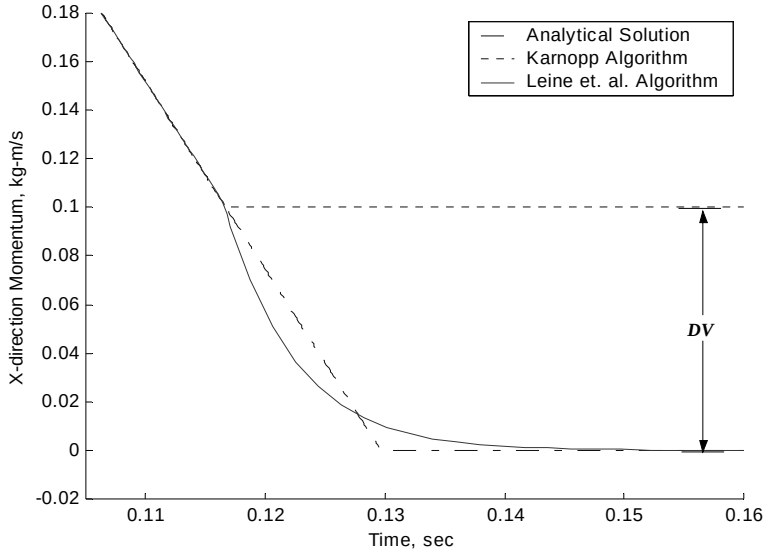

Figure 26. Friction Law Comparison

The behavior of a link sliding to a stop in contact with the CVT pulley is shown in Figure 26. In the slip regime, all solutions are identical. At the transition to stick, the Coulomb solution continues to zero velocity, the Karnopp solution remains at the small

velocity *DV* = 0.1 m/s, and the solution of Leine et. al. converges to zero under the action of a fictitious sticking force.

An additional benefit to a slip stick algorithm is that at velocities under *DV*, all forces other than the fictitious sticking force are cancelled. Canceling these excitations eliminates the numerical instabilities associated with compliant contact modeling, as discussed in the section titled *Contact Model Description and Validation.* The friction model that is validated and used in the dynamic chain CVT simulation is the model of Leine et al.

FRICTION MODEL VALIDATION - The friction model is validated by comparison to analytical solutions using strict Coulomb friction. The first validation test is performed by giving a 2-DOF chain link model an initial velocity and allowing dynamic friction to drag the link to a stop. The chain link is constrained by reaction forces from a pulley model of infinite radius and the applied force of gravity as shown in Figure 27. A comparison of the friction model to the analytical solution is presented graphically in Figure 26.

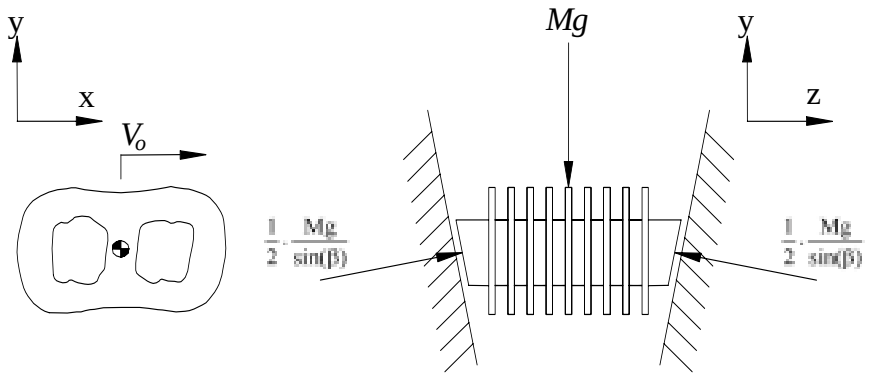

Figure 27. Chain Link Contact Configuration

The comparison shows that the friction model is equivalent to the analytical solution until the sticking velocity is reached. The quantity *DV* must therefore be chosen to be lower than any velocity of interest.

The second validation for the friction model ensures that the friction model is behaving as expected under dynamic slip-stick conditions. To validate the model dynamically, a slip-stick oscillator is simulated with the configuration shown in Figure 28.

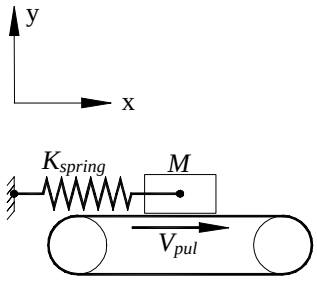

Figure 28. Slip Stick Oscillator

Table 4. Slip Stick Oscillator Operating Conditions

Variable	Symbol	Value
Link Mass	M	1 kg
Coeff. of Static Friction	μ_s	0.18
Coeff. of Dynamic Friction	μ_d	0.15
Linear Spring Constant	K_{spring}	50 N/m
Pulley Velocity	V_{pul}	0.51 m/s
Pulley Half Angle	β	11 deg

Forces imposed on the chain element simulate contact with a CVT pulley of zero curvature as shown in Figure 27. Movement of the chain element is allow in both the x and y directions. Figure 29 shows the trajectory in the x direction of the slip-stick oscillator for one cycle.

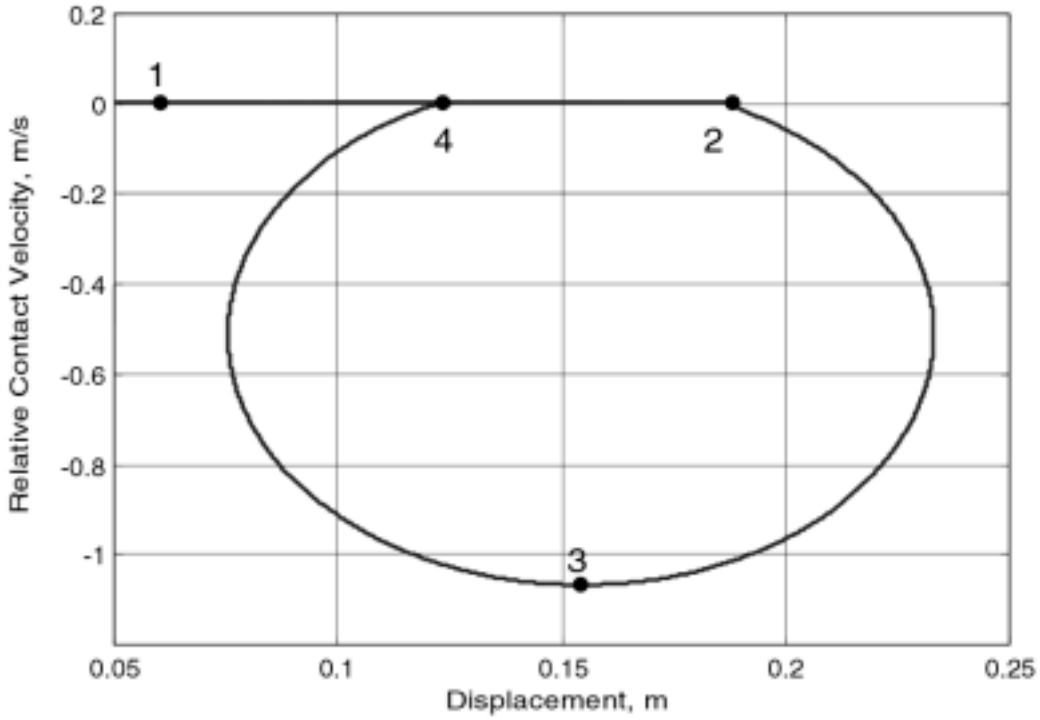

Figure 29. Slip Stick Oscillator Trajectory

From point 1 to point 2, the link is stuck to the moving surface. The relative velocity of the link to the surface is zero and the displacement of the link is increasing at a rate of V_{pul}. At point 2, the force from the displaced spring is equal to the force of static friction, and the link begins to slip relative to the moving surface. Analytically, using Coulomb's law of friction this transition from stick to slip should occur at a displacement of:

$$x = \frac{Mg}{\sin(\beta)} \frac{\mu_s}{K_{spring}} = 0.185m.$$

Numerically, this transition occurs at 0.188*m*. At point 3, the relative and absolute acceleration of the link is zero. Again, from Coulomb's law of friction,

$$x = \frac{Mg}{\sin(\beta)} \frac{\mu_d}{K_{spring}} = 0.154m$$

Numerically, this state occurs at a position of $0.154m$. At point 4 the link sticks and the cycle repeats. From analysis of the slip-stick oscillator the two-dimensional friction model is validated to the Coulomb friction law. The stability and accuracy of the two-dimensional friction law under slip-stick conditions and under conditions of continuous contact is also verified.

Modeled Link and Pulley Characteristics

The link element and pulley characteristics are chosen to emulate the GCI 2L CVT chain installed in a Nissan 2L CVT. Inertias and masses for the links and pulleys are measured or calculated from the actual components. Compliances for the system are calculated from the models of the contacts in the system. Tension in the CVT chain is produced by varying the spacing between the two sheaves of the CVT pulley. Pulleys are rigid and un-skewed. Pulley rigidity is an important simplification because pulley flex and skew determine the dynamics of the chain in contact with the pulley. For proper modeling of the dynamics of the chain in contact with the pulleys, a model of pulley deformation is required [Gerbert 1996; Srnik 1997; Srnik 1999]. Here, this simplification is justified because the focus of this model is chain span dynamics instead of chain/pulley interactions or dynamics.

The models for the 75 element chain and two CVT pulleys are then assembled into a global mathematical model of the CVT variator (CVT chain and pulley system).

Mathematical Formulation

Formulation of Equations

To formulate equations, definitions of the applicable coordinate systems are required. Local coordinate systems are established for each chain element, and a global Newtonian coordinate frame is established. In the most general representation, the model is formulated in the form of equations of motion in the global coordinate frame.

$$[M]\cdot[\ddot{q}]+[h(q,\dot{q})]+[\lambda(q,\dot{q})]=0 \qquad \in \Re^N$$

Where $[M]$ is the positive definite mass matrix for the set of minimal coordinates $[q]$, in the global coordinate system. The vector of states, $[q]$, is of the form

$$[q]=\left[x_1 \quad \Lambda \quad x_{n\_links} \quad y_1 \quad \Lambda \quad y_{n\_links} \quad \theta_1 \quad \Lambda \quad \theta_{n\_links} \quad \theta_{pulley_i} \quad \dot{\theta}_{pulley_i}\right]^T.$$

The vector $[h]$ represents the applied forces due to inter-element reactions and $[\lambda]$ is the vector of applied forces due to contact with the pulleys. Inter-element forces are calculated based on the relative positions and velocities of the chain elements in the global coordinate system. Pulley contact forces, including both friction and unilateral compliance forces, are calculated using a set of vectors normal and tangential to the pulley contact surface. The forces in the tangential and normal directions are coupled via the friction law [Pfeiffer 1996]. The forces normal and tangential to the pulley contact surface are transformed into the global coordinate system and are incorporated into $[\lambda]$. Finally, to represent the action of the involute inter-element contact surface, the position of the inter-element contact is calculated

from the relative angular displacements of adjacent elements. By using a constant causality friction law and an explicit compliant contact modeling scheme, formulation of these equations results in a system of 454 first-order ordinary differential equations.

Solver

The resultant system has eigenvectors corresponding to three main modes: inter-element dynamics, contact dynamics and global chain span dynamics. The eigenvalues of the contact dynamics are roughly of the same order of magnitude as those of the inter-element dynamics. Although the eigenvalues of the global chain span dynamics are significantly slower than the inter-element dynamics, because some portion of the chain is in contact at all times, the time step must always be on the order of the contact dynamics time constant. The system is solved using a 4^{th} order Runge-Kutta scheme of constant step size. A higher order Runge-Kutta algorithm is advantageous because it allows large step sizes while maintaining stability and low error [Nikravesh 1988]. Constant step size is less computationally costly because the magnitude of the contact dynamic eigenvalue does not change significantly over the course of the simulation.

The MATLAB m-files programs and functions that perform the simulations are included in Appendix 2. The program was run in MATLAB 6.1 in the Windows XP operating system using a 2.2 GHz Pentium processor.

Simulation Evaluation Methods

All simulation results presented here are performed with the operating conditions specified in Table 5.

Table 5. Simulation Parameters for Dynamic Model

Parameter	Value	Units
Equivalent Secondary Pressure	243	[psi]
Linear Chain Speed	2.34±0.18	[m/s]
Chain Element Mass	0.031	[kg]
Chain Pitch (Uncurved)	0.00933	[m]
Base Radius (*Rb*): Involute Chain	0.056	[m]
Base Radius (*Rb*): Pinned Chain[2]	0.0	[m]
Dynamic Coefficient of Friction, μ_d	0.2	[-]
Static Coefficient of Friction, μ_s	0.21	[-]

To evaluate the effectiveness of the involute chain design in reducing polygonal action, a dynamic chain model was created of both the pinned contact chain and the involute contact chain. This allows analysis and comparison of the behavior of the chains as a component of the CVT system. The involute contact surface CVT chain that is modeled in this simulation is a close approximation of the 30mm GCI chain as designed for the Nissan 2L CVT. The pinned contact chain is identical in geometry to the involute chain including the initial inter-element contact position, but incorporates 1-D pinned inter-element contacts.

Initially, the very low contact compliance between the chain pins and the pulleys made the equations of the CVT chain system very stiff. Proper clamping pressure could not be maintained. By reducing the stiffness of the pin of the CVT chain, the equations could be made less stiff and the solutions more valid. This compromise will have minor effects on the solutions of the dynamic CVT simulation.

[2]The only difference in geometry between the involute contact chain and the pinned contact chain is *Rb*. Because the vector position of the contact point for each element is modeled as the sum of the vector from the CG to the point of pinned contact plus the vector from the equation of the involute, an involute contact with *Rb* of 0 is equivalent to a pinned contact (see Figure 8).

In general, reduced pin stiffness will exaggerate the radial movement of the CVT chain while in contact with the pulleys. A better solution is to implement a model of the CVT pulley deflection, but this could not be accomplished with validity because of time constraints.

Results and Discussion

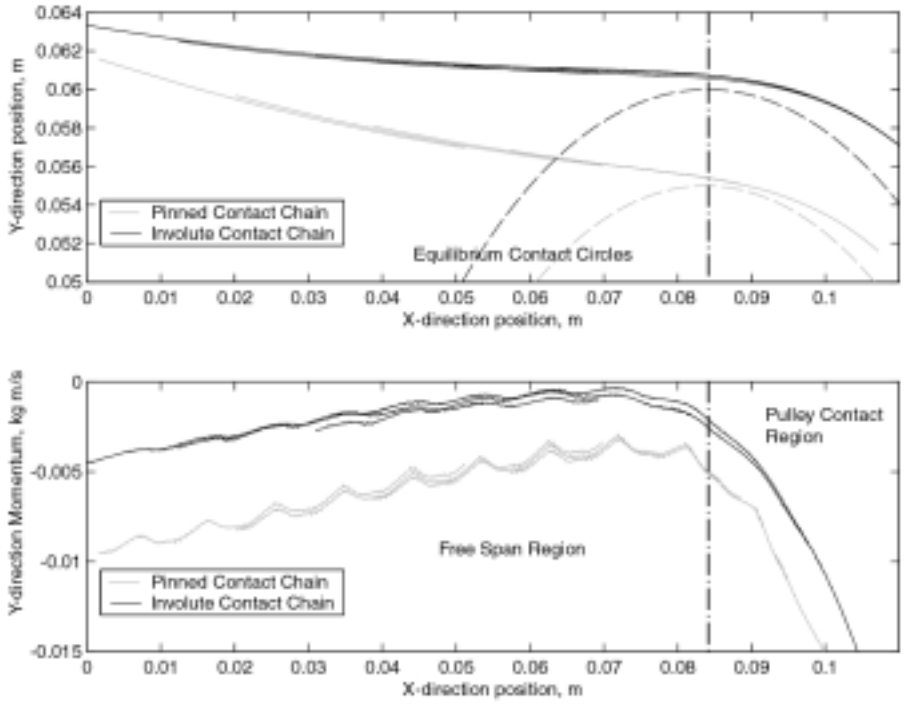

Figure 30. Chain Element Motion at Pulley Entrance

Figure 30 shows a comparison of the chain span motion at entrance to the pulley. The top of Figure 30 is a spatial illustration of the chain path for the involute and pinned contact chains. The bottom of Figure 30 shares the same spatial x-axis as the top of the figure, but the y-axis represents the y-direction momentum of the chain links. Multiple paths are visible in the figure because it is made up of the paths of multiple chain elements and some inter-element variation is present. The entrance to the CVT pulleys is divided into a free span region and a pulley contact region. The

free span region is the portion of the chain path where the chain elements are not in contact with the CVT pulleys. In the pulley contact region, the chain elements make and remain in contact with the pulley.

The dynamic chain path as illustrated in the top half of Figure 30 shows the difference between the pinned contact chain and the involute contact chain. The path of the pinned contact chain is higher dynamically than the path of the involute contact chain. This is qualitatively consistent with the results of the static models, but secondary factors exaggerate this effect in the dynamic simulation. One such factor is that although the models of the two chains have the same number of elements and the same chain pitch, the length of the chains are different. When curved, the length of the involute chain gets longer due to the rolling motion of the contact surfaces. This is not true of the pinned contact chain. As such, the involute chain is longer than the pinned chain and occupies a larger equilibrium radius when in contact with the pulleys. This cannot account for all of the difference observed, and it must be concluded that the difference in chain structure causes the chains to follow different paths at entrance to the pulleys. The pulley to chain contact conditions and behavior is an aspect of this dynamic simulation that is very sensitive to the values assigned to contact compliances, coefficients of friction and other parameters. Further validation is necessary to allow for quantitative analysis of the pulley to chain contact. For reference, a visual comparison of the chain paths at larger scale is shown in Figure 31 and Figure 32.

The difference between the momenta near pulley entrance of the involute chain and the pinned chain is shown in the bottom half of Figure 30. As both chains

approach the pulley, until they make contact near *x_e = 0.084 m*, they are acted on by contact forces due to polygonal action. These forces accelerate the links in the *y_e* direction, and result in the cyclic pattern of momentum change illustrated in Figure 30. The length of each cycle in the *x_e* direction is 9.33 mm, the pitch of both chains. The difference between the behavior of the two chain types is visible in the shape and magnitude of the cycles of momentum change. The magnitude of the cycles and the rates of change of momentum are much lower in the involute chain indicating less chain vibration at pulley entrance and a reduction in polygonal action.

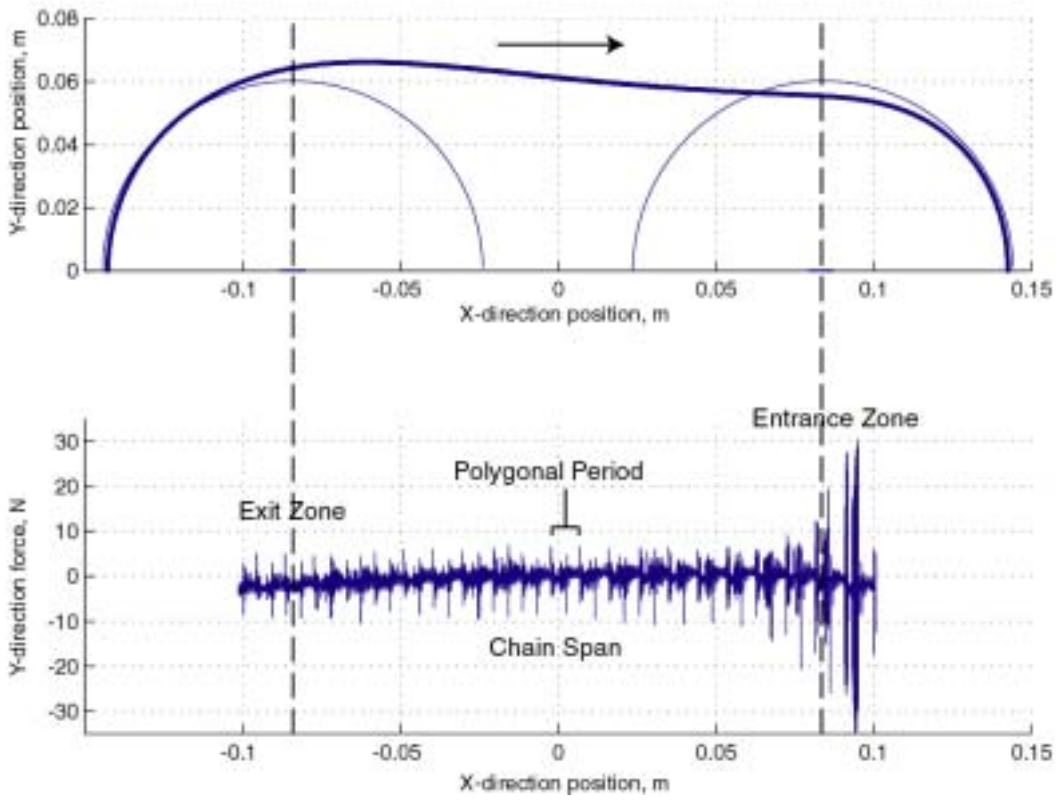

Figure 31. Pinned Contact Chain Span Motion

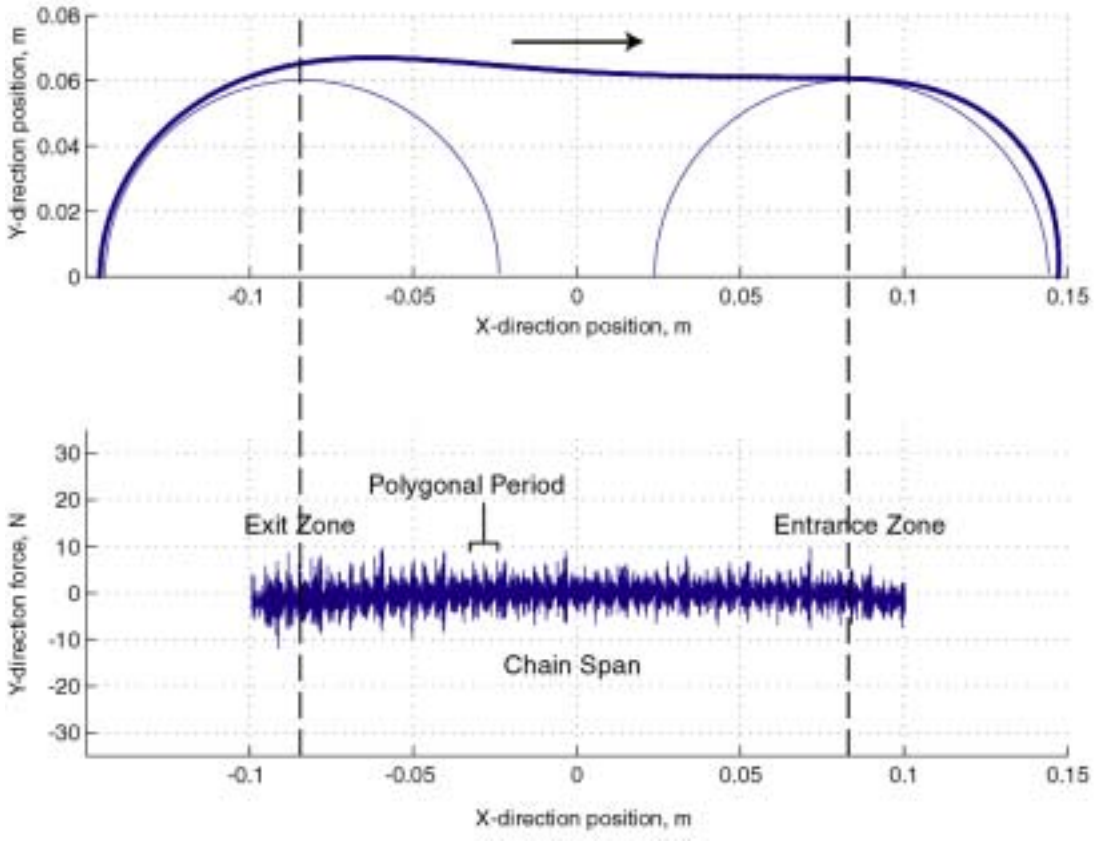

Figure 32. Involute Contact Chain Span Motion

Figure 31 and Figure 32 show the chain span shape and the forces normal to the path of the chain over the entire chain span. The dynamic path of the chain elements is shown in the top halves of the figures. The two circles serve as references to identify the location of the two CVT pulleys. In both figures, the circles are of 60.5 mm radius and correspond roughly to the equilibrium contact circle of both chains. The bottom half of each figure shows the forces in the *y_e* direction experienced by each chain element as a function of its position in the chain span. The *y_e* direction is roughly perpendicular to the chain path so forces in the *y_e* direction generate vertical chain span vibration.

Again, the top halves of Figure 31 and Figure 32 show the chain path for the two chain types. Because the simulation is performed with no torque transmitted, the

chain path is symmetrical about the *x_e* axis. Here it is evident that although both chains have different paths near the pulley entrance, they both settle to near the equilibrium radius of 60.5 mm before exiting the pulley.

Comparison of the *y_e* direction force experienced by the chain elements shows very different behavior between the two chain types. The dramatic increase in forces that is experienced by the pinned contact chain as the links make contact with the pulley at *x_e* = 0.084 m is not visible in the involute contact chain. This indicates much lower polygonal action. Also notable is the fact that no large forces exist where the chain span exits from the CVT pulley. This suggests that although exit effects do contribute to the dynamic chain span shape, they do not impart very large forces perpendicular to the chain path. A qualitative difference in the magnitude of the forces associated with polygonal action can also be seen. Polygonal forces can be identified in both Figure 31 and Figure 32 because they occur at intervals of 0.00933 m, the pitch of both chains. These forces are caused by transmission through the chain span of impact forces from contact of the chain pins with the pulley.

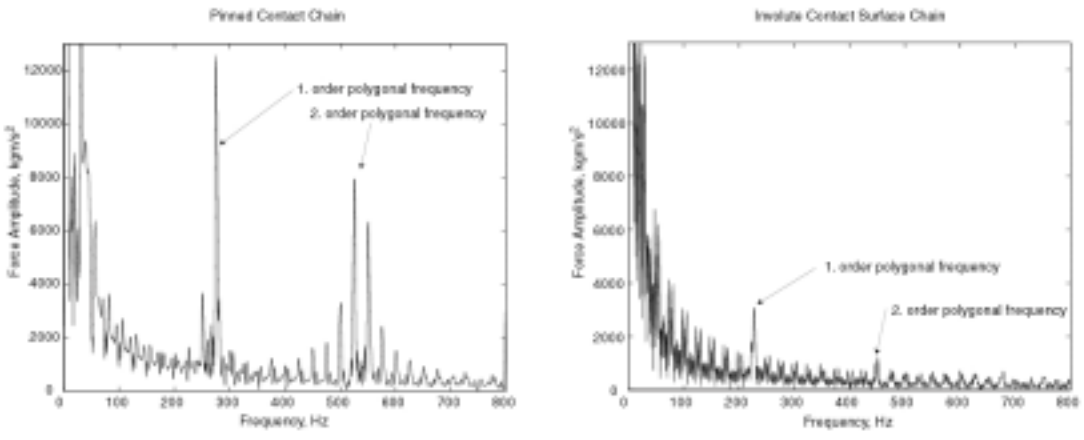

Figure 33. Frequency Spectra for Pinned and Involute Contact Chains

Spectral analysis of the vibration of the chain elements in the chain span provides for a more quantitative comparison. The spectra of the forces in the *y_e* direction that are applied to the chain elements as they travel along the chain span are presented in Figure 33. In these simulations the polygonal frequency of the involute contact chain and the pinned contact chain are 231 Hz and 270 Hz respectively. The difference in frequency is present because of a difference in pulley speeds, and slip rates between the two chain designs. In both chains, both the first and second order polygonal frequency are evident, but the magnitude of the excitations at the polygonal frequencies is much greater for the pinned contact chain. Lower magnitudes for the involute contact chain indicate a reduction in vibrations from polygonal action.

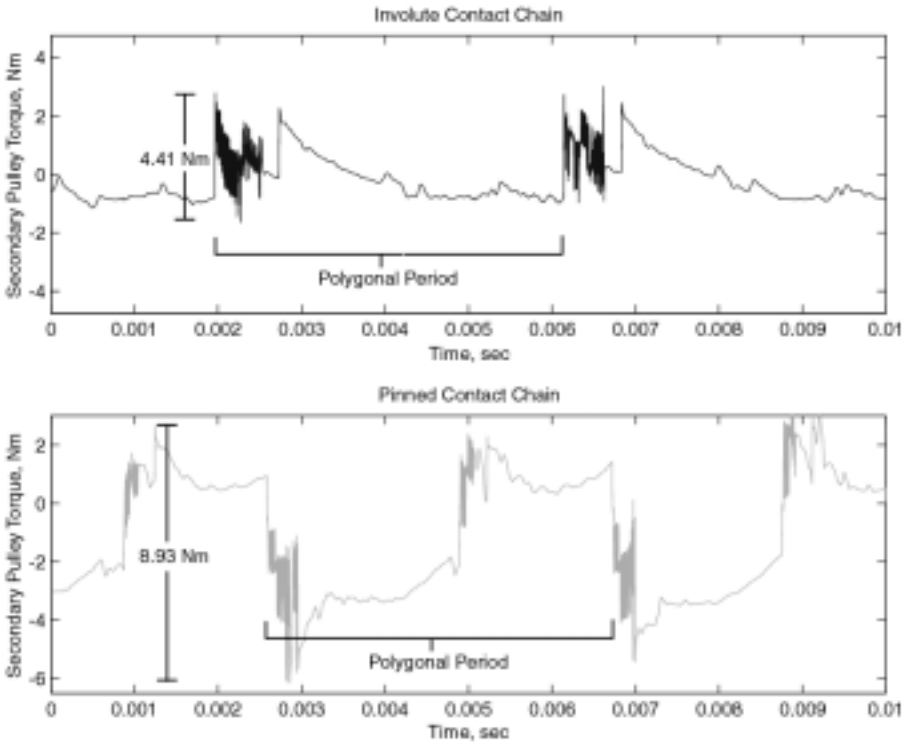

Figure 34. Secondary Pulley Torque Profile

The reduction in polygonal action that is present in the involute contact chain has influences on the entire CVT system, not just the chain span. As shown in Figure

34, the reduction in polygonal action more than halves the peak-to-peak torque fluctuations that are transmitted to the CVT pulleys. This has the additional effect of lessening the vibrations passed to other components of the drivetrain.

DYNAMIC MODELING CONCLUSIONS - The results of the dynamic model show that there is a significant improvement in the vibration behavior of the involute contact CVT chain when compared to the pinned contact chain. Polygonal excitation of both the chain span and the CVT pulleys are significantly decreased, providing further justification of the involute chain design concept. Exit effects are shown to play a minor role in polygonal excitation of the CVT chain span

CONCLUSIONS AND RECOMMENDATIONS

Static and dynamic models have been presented to analyze and simulate the dynamics of CVT chains. The models presented show the ability to simulate polygonal action in CVT chains and CVT variators.

The static models developed here have been used as a tool for design of the inter-element contact surfaces. Specifically the discrete static model is used to analyze the tradeoffs present in design of these contact surfaces. Results of the static model can be used to predict and minimize polygonal action by solving for *dh* and pin-to-pulley angle of incidence as a function of pulley radius. Results from the static models show that, with proper design, CVT chains with involute inter-element contact surfaces display less static mid-span displacement, smaller angle of incidence at impact and they impact the pulley closer to tangent, when compared to pinned contact point CVT chains. This behavior is predictive of reduced polygonal action and the lower vibration, higher efficiency and lower sound emissions that generally accompany that reduction.

Dynamic models were constructed to analyze polygonal action dynamically and at the CVT system-level. A scheme of 2-D compliant contact modeling with an explicit slip-stick friction law was developed and implemented in this model. With the dynamic model the forces on the chain elements and on the CVT pulleys can be predicted and compared for chains of various designs. Non-linear dynamic effects of polygonal action can be predicted and incorporated into CVT chain design. Results from the dynamic models show that the involute contact surface chain experiences lower polygonal forces both at contact and at midspan. Reduced forces cause less

excitation of other vibration frequencies and lower torque pulses to the pulleys and other components of the CVT system. The large magnitude of this reduction indicates that the involute contact surface CVT chain can significantly improve the dynamic characteristics of CVT chains.

Future development should be centered on improvement of the dynamic chain model. Further work is needed to improve the applicability of the model and perform a detailed validation of the model as a whole. The implementation of the compliant contact modeling scheme with explicit friction modeling is somewhat of a success although stability problems demand more refinement. Simulation of various speed and loading conditions will allow for a more detailed investigation of the dynamic behavior of the involute chain CVT. Modeling of pulley skew and deflection will improve the stability and validity of the simulation, especially for predicting the behavior of the chain when in contact with the pulleys. The results of this research are best viewed as a comparison between the involute and pinned contact chain simulations because of incomplete model validation. Dynamic simulations are best validated with experimental results. Experimental acoustic and dynamic testing of CVT chains would provide a basis for further refinement of the dynamic chain models.

REFERENCES

Abadie, M. (2000). Dynamic Simulation of Rigid Bodies: Modeling of Frictional Contact. Impacts in Mechanical Systems - Analysis and Modeling. B. Brogliato. Berlin, Springer Verlag**:** 61-144.

Abo, K., Kobayashi, M. (2000). "Development of a new metal-belt CVT for high-torque engines." Society of Automotive Engineers Technical Paper Series, 2000-01-0829.

Ariaratnam, S. T., Asokanthan, S. F. (1987). "Dynamic stability of chain drives." Journal of Mechanisms, Transmission and Automation in Design **109**: 412-418.

Avramidis, S. (1986). "A "state of the art" chain driven CVT design." Society of Automotive Engineers Technical Paper Series, 861354.

Bothwell, S. L. (1987). Investigation of Chain Dynamics with Application to Noise. Department of Mechanical and Aeronautical Engineering, University of California, Davis**:** 51.

Bradley, T. H., Huff, B. R., Frank, A. A. (2002). Test and Evaluation of the UC Davis Servo-Hydraulic CVT Control System and the GCI CVT Chain in a Hybrid Electric Vehicle: A Report To Nissan Motor Company, University of California, Davis**:** 81.

Brandsma, A., van Lith, J., Hendricks, E. (1999). Push belt CVT developments for high power applications. International Congress on Continuously Variable Power Transmission, Eindhoven, Netherlands.

Fujii, T., Kurokawa, T. (1993). "A study of a metal pushing v-belt type CVT - Part 1: Relation between transmitted torque and pulley thrust." Society of Automotive Engineers Technical Paper Series, 930666.

Gerbert, G. (1984). "Metal v-belt mechanics." ASME Paper **84-DET-227**.

Gerbert, G. (1996). Skew v-belt pulleys. International Conference on Continuously Variable Power Transmission, Yokohama, Japan, Japan Society of Automotive Engineers.

Hendricks, E. (1993). "Qualitative and quantitative influence of a fully electronically controlled CVT on fuel economy and vehicle performance." Society of Automotive Engineers Technical Paper Series, 930668.

Hirano, S., Miller, A. L., Schneider, K. F. (1991). "SCVT - A state of the art electronically controlled continuously variable transmission." Society of Automotive Engineers Technical Paper Series, 910410.

Ide, T. (2000). Effect of belt loss and oil pump loss on the fuel efficiency of a vehicle with a metal v-belt CVT. FISITA World Automotive Congress, Seoul, Korea.

Johnson, K. L. (1985). Contact Mechanics. Cambridge, Cambridge University Press.

Karnopp, D. (1985). "Computer simulation of stick-slip friction in mechanical dynamic systems." Journal of Dynamic Systems, Measurement, and Control **107**: 101.

Khiralla, T. F. (1976). On the Geometry of External Involute Spur Gears. North Hollywood, California, C/I Leaming.

Kluger, M. A., Long, D. M. (1999). "An overview of current automatic, manual and continuously variable transmission efficiencies and their projected future

improvements." Society of Automotive Engineers Technical Paper Series, 1999-01-1259.

Kobayashi, D., Mabuchi, Y., Katoh, Y. (1998). "A study on the torque capacity of a metal pushing v-belt for CVTs." Society of Automotive Engineers Technical Paper Series, 980822.

Kraus, P. R., Kumar, V. (1997). Compliant Contact Models for Rigid Body Collisions. 1997 IEEE International Conference on Robotics and Automation, Albuquerque, New Mexico, IEEE.

Leine, R. I., Van Campen, D. H., De Kraker, A., Van Den Steen, L. (1998). "Stick-slip vibrations induced by alternate friction models." Nonlinear Dynamics **16**: 41-54.

Micklem, J. D., Longmore, D. K., Burrows, C. R. (1994). "Modeling of a steel v-belt continuously variable transmission." Journal of Mechanical Engineering Science **208**: 14-27.

Nikravesh, P. E. (1988). Computer-Aided Analysis of Mechanical Systems. London, Prentice-Hall.

Pfeiffer, F., Glocker, C. (1996). Multibody Dynamics with Unilateral Contacts. New York, Wiley and Sons.

Reeves, M. O. (1897). Speed Varying Mechanism. United States Patent, Reeves Pulley Company.

Sedlmayr, M., Bullinger, M., Pfeiffer, F. (2002). "Spatial dynamics of CVT chain drives." VDI Berichte **1709**.

Srnik, J., Pfeiffer, F. (1994). Simulation of a CVT Chain Drive as a Multibody System with Variant Structure. The First Joint Conference of International Simulation Societies, Zurich, Switzerland.

Srnik, J., Pfeiffer, F. (1997). Dynamics of CVT chain drives: Mechanical model and verification. Design Engineering Technical Conferences, Sacramento, California.

Srnik, J., Pfeiffer, F. (1999). "Dynamics of CVT chain drives." International Journal of Vehicle Design **22**(1).

Stronge, W. J. (2000). "Chain reaction from impact on coaxial multibody systems." Journal of Applied Mechanics **67**: 632-635.

Stronge, W. J. (2000). Contact Problems for Elasto-Plastic Impact in Multi-body Systems. Impacts in Mechanical Systems - Analysis and Modeling. B. Brogliato. Berlin, Springer Verlag**:** 191-234.

Stronge, W. J. (2000). Impact Mechanics, Cambridge University Press.

Takahashi, M., Kido, R., Nonaka, K., Takayama, M., Fujii, T. (1999). Design and development of a dry hybrid belt (BANDO AVANCE) for CVT vehicles. International Congress on Continuously Variable Power Transmission CVT '99, Eindhoven, The Netherlands.

Tanaka, H., Goi, T. (1999). Traction drive of a high speed double cavity half-toroidal CVT. International Congress on Continuously Variable Power Transmission CVT '99, Eindhoven, The Netherlands.

Troedsson, I., Vedmar, L. (2001). "A dynamic analysis of the oscillations in a chain drive." Journal of Mechanical Design **123**: 395-401.

van Rooij, J., Frank, A. (2002). Development of a 700 Nm chain CVT. International Conference on Continuously Variable Power, Munich, Germany.

van Rooij, J. H. M. (1991). Volvo Car's new chain concept. 3rd International EAEC Conference on Vehcile Dynamics and Powertrain Engineering, Strasbourg, France.

van Rooij, J. H. M. (1993). The chain CVT. Year Book Autotechnical Trends. Arnhem, The Netherlands, Hogeschool Geluerland.

van Rooij, J. H. M., Cadee, T. P. M. (1996). Transmission chain for a cone pulley transmission. European Patent, Gear Chain Industrial B. V.

Wagner, U., Teubert, A., Endler, T. (2001). "Entwicklung von CVT-ketten fuer Pkw-anwendungen bis 400 Nm." VDI Berichte(1610).

APPENDIX 1 – Discrete Static CVT Chain Model:

MATLAB M-files

inv.m

```
%inv.m - Discrete static cvt chain model initialization program
%by: Thomas Bradley 9/17/02

clear
global Rad Rb step_in tomout dt_left Q t gamma epsilon


x0 = [0         %Q(2,x) = x0(1);
   .059         %Q(2,y) = x0(2);                              % y_pulley
                %position of the end of A_e of link 1
   -0.00933     %Q(3,x) = x0(3);
   .059         %Q(3,y) = x0(4);
   -0.00933*2   %Q(4,x) = x0(5);
   .059         %Q(4,y) = x0(6);
   -0.00933*3   %Q(5,x) = x0(7);
   .059
   -deg2rad(20)%Q(5,y) = x0(8);
   -deg2rad(15)%t(1) = x0(9);                                 % theta
                %direction position of link 1
   -deg2rad(11)   %t(2) = x0(10);                               % theta
                %direction position of link 2
   -deg2rad(6) %t(3) = x0(11);                                % theta
                %direction position of link 1%
   -deg2rad(2) %t(4) = x0(12);                                % theta
                %direction position of link 1
   -deg2rad(1)
0.2769
-0.0468
]';             %t(5) = x0(13);
                % theta direction position of link 1

radius = [0.0349];%:0.002:0.078];;  % !!!!!!!!!!!!!!!!!!!!

%option 1 --- works

step_theta = -[ 0
   0.15
   0.2116
0.2463
0.2809
0.3155
0.3501
0.3847
0.4193
0.4539
0.4681
.47
```

```
.48];
%option 2
step_theta = -[-0.0082
0.0264
0.0610
0.0957
0.1303
0.1649
0.1995
0.2341
0.2687];


for i = 1:length(radius)
   Rad = radius(i);
   for j = 1:length(step_theta);
      step_in = step_theta(j) ;
      options = optimset('TolFun', 1e-11, 'Display', 'iter',
'Diagnostics', 'on', 'MaxIter', 150 ); % Turn off Display
      [x_out,Fval,exitflag] = fsolve('involute_fxn6',x0 ,options) ;

      x_output(:,j) = [Q(1,:) Q(2,:) Q(3,:) Q(4,:) Q(5,:) Q(6,:)
t(1:6) gamma epsilon]';
     exitflag
      x_output;
      %x_out(:,j) = x';
   end
end

x_output



involute_plotter6
```

involute_fxn6.m

```
function F = involute_fxn6(x0)

global Rad Rb step_in tomout dt_left Q  t gamma epsilon

%involute_fxn6.m - Discrete static cvt chain model iteration program
% called by fsolve.m
%by: Thomas Bradley 9/17/02

x = 1;
y = 2;

Rb = 56.2327*1e-3;%                         % m; %
!!!!!!!!!!!!!!!!!!!!
a = -1.5371;                          % mm; % !!!!!!!!!!!!!!!!!!!!
0;%




%Q(2,x) = x0(1);                            % x_pulley position of the
                                            %end of A_e of link 1
%Q(2,y) = x0(2);                            % y_pulley position of the
                                            %end of A_e of link 1
Q(3,x) = x0(1);                             % x_pulley position of the
                                            %end of A_e of link 1
Q(3,y) = x0(2);                             % y_pulley position of the
                                            %end of A_e of link 1
Q(4,x) = x0(3);
Q(4,y) = x0(4);
Q(5,x) = x0(5);
Q(5,y) = x0(6);
Q(6,x) = x0(7);
Q(6,y) = x0(8);

t(1) = x0(9);                     % theta direction position of link 1
t(2) = x0(10);                    % theta direction position of link 2
t(3) = x0(11);                    % theta direction position of link 1
t(4) = x0(12);                    % theta direction position of link 1
t(5) = x0(13);                    % theta direction position of link 1
t(6) = x0(14);
gamma = x0(15);
epsilon = x0(16);
%d = x0(14);                      % y_pulley direction position of the
                                  %end of A_e of link 1

A_bc = [-5.5269 0]'*1e-3;         % !!!!!!!!!!!!!!!!!!!!
A_b = [-3.7152 a]'*1e-3;          % !!!!!!!!!!!!!!!!!!!!
B_b = [5.6149 a]'*1e-3;           % !!!!!!!!!!!!!!!!!!!!

if Rb == 0
   A_b = [-9.33/2 0]'*1e-3;
   B_b = [9.33/2 0]'*1e-3;
```

```
   A_bc = [-9.33/2 0]'*1e-3;
end

x = 1;
y = 2;

%I need 14 zeros in the Z vector

%%%%%%%%%%%%%%%%%%%%%%%%%%%%%%%%%% for element 1 %%%%%%%%%%%%%%%%%%%%
%option 2
t_p = step_in;
t(1) = step_in + gamma/2 + gamma - 0.04438;


Q(2,x) = -Rad*sin(t_p);
Q(2,y) = Rad*cos(t_p);
Q(1,x) = -Rad*sin(t_p + gamma);        %gamma is (-)
Q(1,y) = Rad*cos(t_p + gamma);


Z(1) = -t(2) + t(1) - gamma;
Z(2) = -gamma - atan2(Q(2,2),Q(2,1)) + atan2(Q(1,2),Q(1,1));


%%%%%%%%%%%%%%

T_1= [cos(t(1)) -sin(t(1)); sin(t(1)) cos(t(1))];
T_2= [cos(t(2)) -sin(t(2)); sin(t(2)) cos(t(2))];
T_3= [cos(t(3)) -sin(t(3)); sin(t(3)) cos(t(3))];
T_4= [cos(t(4)) -sin(t(4)); sin(t(4)) cos(t(4))];
T_5= [cos(t(5)) -sin(t(5)); sin(t(5)) cos(t(5))];
T_6= [cos(t(6)) -sin(t(6)); sin(t(6)) cos(t(6))];

%%%%%%%%%%%%%%%%%%%%%%%%%%%%%%%%%% element 1 & 2 %%%%%%%%%%%%%%%%%%%%

i = 2;
A_ec_left = T_2*A_bc;
A_e_left = T_2*A_b;
B_e_left = T_2*B_b;
A_e_right = T_1*A_b;
B_e_right = T_1*B_b;
A_ec_right = T_1*A_bc;

dt_left = (t(i) - t(i+1));
x_t_left = -Rb*sin(-dt_left) + Rb*(-dt_left)*cos(-dt_left);
y_t_left =  Rb*cos(-dt_left) + Rb*(-dt_left)*sin(-dt_left)-Rb;
if dt_left >= 0
   x_t_left = 0;
   y_t_left = 0;
end

dt_right = (-t(i) + t(i-1));
x_t_right= -Rb*sin(-dt_right) + Rb*(-dt_right)*cos(-dt_right);
y_t_right=  Rb*cos(-dt_right) + Rb*(-dt_right)*sin(-dt_right)-Rb;
if dt_right >= 0
   x_t_right = 0;
   y_t_right = 0;
```

```
end



Z(3:4) = Q(2,:)' + T_2*(- A_bc + B_b + [0 1/2*Rb*dt_right^2]')...
   -(Q(1,:)' + T_1*(- A_bc + A_b + [x_t_right; y_t_right]));


tomout(2) = Q(2,y) -A_ec_left(y) + A_e_left(y) + [0 1] *
(T_2*[x_t_left; y_t_left]);
tomout(1) = (Q(1,y) - A_ec_right(y) + A_e_right(y) + [0 1] *
(T_1*[x_t_right; y_t_right]));

%%%%%%%%%%%%%%%%%%%%%%%%%%%%%%%%% element 2 & 3 %%%%%%%%%%%%%%%%%%%%

i = 3;
A_ec_left = T_3*A_bc;
A_e_left = T_3*A_b;
B_e_left = T_3*B_b;
A_e_right = T_2*A_b;
B_e_right = T_2*B_b;
A_ec_right = T_2*A_bc;

dt_left = (t(i) - t(i+1));
x_t_left = -Rb*sin(-dt_left) + Rb*(-dt_left)*cos(-dt_left);
y_t_left =  Rb*cos(-dt_left) + Rb*(-dt_left)*sin(-dt_left)-Rb;
if dt_left >= 0
   x_t_left = 0;
   y_t_left = 0;
end

dt_right = (-t(i) + t(i-1));
x_t_right = -Rb*sin(-dt_right) + Rb*(-dt_right)*cos(-dt_right);
y_t_right =  Rb*cos(-dt_right) + Rb*(-dt_right)*sin(-dt_right)-Rb;
if dt_right >= 0
   x_t_right = 0;
   y_t_right = 0;
end

Z(5) = [0 1]*(Q(3,:)' + T_3*(- A_bc + A_b + [x_t_left; y_t_left])-
(Q(2,:)' + T_2*(- A_bc + A_b + [x_t_right; y_t_right])));

Z(6:7) = Q(3,:)' + T_3*(- A_bc + B_b + [0 1/2*Rb*dt_right^2]')...
   -(Q(2,:)' + T_2*(- A_bc + A_b + [x_t_right; y_t_right]));



tomout(3) = Q(3,y) -A_ec_left(y) + A_e_left(y) + [0 1] *
(T_3*[x_t_left; y_t_left]);

%%%%%%%%%%%%%%%%%%%%%%%%%%%%%%%%% element 3 & 4 %%%%%%%%%%%%%%%%%%%%
i = 4;
A_ec_left = T_4*A_bc;
A_e_left = T_4*A_b;
B_e_left = T_4*B_b;
A_e_right = T_3*A_b;
```

```
B_e_right = T_3*B_b;
A_ec_right = T_3*A_bc;

dt_left = (t(i) - t(i+1));
x_t_left = -Rb*sin(-dt_left) + Rb*(-dt_left)*cos(-dt_left);
y_t_left =  Rb*cos(-dt_left) + Rb*(-dt_left)*sin(-dt_left) - Rb;
if dt_left >= 0
   x_t_left = 0;
   y_t_left = 0;
end

dt_right = (-t(i) + t(i-1));
x_t_right = -Rb*sin(-dt_right) + Rb*(-dt_right)*cos(-dt_right) ;
y_t_right =  Rb*cos(-dt_right) + Rb*(-dt_right)*sin(-dt_right)-Rb;
if dt_right >= 0
   x_t_right = 0;
   y_t_right = 0;
end

Z(8) = [0 1]*(Q(4,:)' + T_4*(- A_bc + A_b + [x_t_left; y_t_left])-
(Q(3,:)' + T_3*(- A_bc + A_b + [x_t_right; y_t_right])));

Z(9:10) = Q(4,:)' + T_4*(- A_bc + B_b + [0 1/2*Rb*dt_right^2]')...
   -(Q(3,:)' + T_3*(- A_bc + A_b + [x_t_right; y_t_right]));


tomout(4) = Q(4,y) -A_ec_left(y) + A_e_left(y) + [0 1] *
(T_4*[x_t_left; y_t_left]);

%%%%%%%%%%%%%%%%%%%%%%%%%%%%%%%%% element 4 & 5 %%%%%%%%%%%%%%%%%%%%
i = 5;
A_ec_left = T_5*A_bc;
A_e_left = T_5*A_b;
B_e_left = T_5*B_b;
A_e_right = T_4*A_b;
B_e_right = T_4*B_b;
A_ec_right = T_4*A_bc;


dt_left = (t(i) - t(i+1));
x_t_left = -Rb*sin(-dt_left) + Rb*(-dt_left)*cos(-dt_left);
y_t_left =  Rb*cos(-dt_left) + Rb*(-dt_left)*sin(-dt_left)-Rb;
if dt_left >= 0
   x_t_left = 0;
   y_t_left = 0;
end

dt_right = (-t(i) + t(i-1));
x_t_right = -Rb*sin(-dt_right) + Rb*(-dt_right)*cos(-dt_right);
y_t_right =  Rb*cos(-dt_right) + Rb*(-dt_right)*sin(-dt_right)-Rb;
if dt_right >= 0
   x_t_right = 0;
   y_t_right = 0;
end

Z(11) = [0 1]*(Q(5,:)' + T_5*(- A_bc + A_b + [x_t_left; y_t_left])-
(Q(4,:)' + T_4*(- A_bc + A_b + [x_t_right; y_t_right])));
```

```
Z(12:13) = Q(5,:)' + T_5*(- A_bc + B_b + [0 1/2*Rb*dt_right^2]')...
   -(Q(4,:)' + T_4*(- A_bc + A_b + [x_t_right; y_t_right]));



tomout(5) = Q(5,y) -A_ec_left(y) + A_e_left(y) + [0 1] *
(T_5*[x_t_left; y_t_left]);

%%%%%%%%%%%%%%%%%%%%%%%%%%%%%%%%% element 5 & 6 %%%%%%%%%%%%%%%%%%%%
i = 6;
A_ec_left = T_6*A_bc;
A_e_left = T_6*A_b;
B_e_left = T_6*B_b;
A_e_right = T_5*A_b;
B_e_right = T_5*B_b;
A_ec_right = T_5*A_bc;
t(7) = 0;

dt_left = (t(i) - t(i+1));
x_t_left = -Rb*sin(-dt_left) + Rb*(-dt_left)*cos(-dt_left);
y_t_left =  Rb*cos(-dt_left) + Rb*(-dt_left)*sin(-dt_left)-Rb;
if dt_left >= 0
   x_t_left = 0;
   y_t_left = 0;
end

dt_right = (-t(i) + t(i-1));
x_t_right = -Rb*sin(-dt_right) + Rb*(-dt_right)*cos(-dt_right);
y_t_right =  Rb*cos(-dt_right) + Rb*(-dt_right)*sin(-dt_right)-Rb;
if dt_right >= 0
   x_t_right = 0;
   y_t_right = 0;
end

Z(14) = [0 1]*(Q(6,:)' + T_6*(- A_bc + A_b + [x_t_left; y_t_left])-
(Q(5,:)' + T_5*(- A_bc + A_b + [x_t_right; y_t_right])));
Z(15:16) = Q(6,:)' + T_6*(- A_bc + B_b + [0 1/2*Rb*dt_right^2]')...
   -(Q(5,:)' + T_5*(- A_bc + A_b + [x_t_right; y_t_right]));



tomout(6) = Q(6,y) -A_ec_left(y) + A_e_left(y) + [0 1] *
(T_6*[x_t_left; y_t_left]);

%%%%%%%%%%%%%%%%%%%%%%%%%%%%%%%%%

F = Z';
```

APPENDIX 2 – Dynamic CVT Chain Model:

MATLAB M-files

chain_init_v13f.m

```
% chain_init.m
% This m-file determines the initial locations of the links at a 1:1
%  ratio, and initializes the Runge Kutta solver
% Thomas Bradley 7/8/01
disp('Running - gci_init_v13f.m')
for n_times = 1:1
format compact
tic
clear

global c2c l_link n_links A_b B_b r K_b C_b M center1 center2
global pulley_beta contact_flag force_comp w_p U C_mat A_mat
global A_e B_e h step contact_flag_out dYdt_pre t_end K_e C_e R
global F_clamp K_link w_link z0 F_t F_n e_v_contactt
global mu_s mu_d e_F_l e_t_l e_n_l r_pulley dist_c e_r_sigp e_n_p
global m_out e_v_contactn m  e_t_p U_out dYdt_1 Z
global I_link t_end_last J_pulley Z_out Y_test contact_flag2 cf_out
global pulley_i A_ec Z_last A_bc B_bc e_v_contact_tangential
global e_v_pullc

plotting = 0;
disp('Link Position Initialization...')
disp('Overall Length Error, mm')

start_over = 0%<------------------------------- this is the restart

if start_over == 0
   load chain_output21_29
   size_buff = size(Y_out);
   Y0 = Y_out(size_buff(1),:);
   n_links = 75;           % # of links
   r = 59.3                % r is the 1:1 radius of the chain; (mm)


elseif start_over == 2
   done = 0;
   c2c = 167.99e-3;        % Nissan 2L CVT center to center pulley
                           %distance (m)
   l_link = 9.33/1000;     % GCI link length (m)
   r = 59.3e-3 ;           % r is the 1:1 radius of the chain; (mm)
   n_links = floor(2*pi*r/.00925);
   angle = [0:2*pi/n_links:(2*pi-2*pi/n_links)];
   x_init = sin(angle) * r;
   y_init = cos(angle) * r;
   theta_init = -angle+2*pi;
   for i = 1:length(theta_init)
```

```
      if theta_init(i) <= -pi;
         theta_init(i) = theta_init(i) +  2*pi;
      end
   end

   x_dot_init = zeros(1,n_links);
   y_dot_init = zeros(1,n_links);
   theta_dot_init = zeros(1,n_links);
   Y0 = [(x_init-c2c/2) y_init theta_init x_dot_init y_dot_init
theta_dot_init 0 0.001 0 0];

   load gci_output6_5
   size_buff = size(Y_out);
   Y0 = Y_out(size_buff(1),:);
   clear Y_out

elseif start_over == 1
   c2c = 167.99;           % Nissan 2L CVT center to center pulley
                           %  distance (mm)
   l_link = 9.29           % GCI link length (mm) est.
   n_links = 75;           % # of links
   r = 56;                 % r is the 1:1 radius of the chain; (mm)
   done = 0;
   while done == 0
      x = zeros(n_links,2);      % vector of link positions, has the
                                 %  form [x y] (mm)
      x(1,:) = [-c2c/2 r];       % this establishes the position of
                                 %  the 1st pin (mm)
      top = 1;                   % this flag goes off when the
                                 %  program is assigning the
                                 %  position of the links on the
                                 %  bottom of the chain
      through = 0;
      thru = 0;
      for i=2:76
         if top == 1
                  % corresponds to section 1 and 2 of the chain.  p9
            x(i,:) = x(i-1,:)+[l_link 0];
            if x(i,1) >= c2c/2
                  % corresponds to section 2 of the chain.  p9
               xbuff = zeros(1,2);
               xbuff(1,:) = x(i-1,:) - [c2c/2 0];
                  % xbuff holds the position of the previous link
                  %  where the pulley is centered at the origin
               [x2,y2] = solve('l_link = sqrt((xbuff(1,1) -
x2)^2+(xbuff(1,2)-y2)^2)','r^2 = x2^2+y2^2');
                  % solves the equation for where the pulley
                  %  diameter and the link length interesect
               x(i,1) = max(eval(x2))+c2c/2 ;
                                 % going clockwise the rightmost x
                                 %  coord and the lowest
                                 %  y coord should be taken
               x(i,2) = min(eval(y2));
               if x(i,2) <=0
                  buff_dude = (eval(x2))+c2c/2;
                  x(i,1) = buff_dude(2);
                                 % when you round the corner the
```

```
                                %  leftmost x coord
               end
            end
            if (x(i,2)-x(i-1,2)) > 0
               top = 0;          % if the link begins to move
                                 %  upwards around the circle
                                 %  then the not_top regime has been
                                 %  reached
            end
         end
         if (top == 0)
            xbuff = zeros(1,2);
            xbuff(1,:) = x(i-1,:) - [c2c/2 0];
            [x2] = solve('l_link = sqrt((xbuff(1,1) -
x2)^2+(xbuff(1,2)-r)^2)');
            x(i,1) = min(eval(x2))+c2c/2 ;
         end

         if and((x(i,2)-x(i-1,2)) >= 0, top == 0)
                                 % if it is not in the top regime
                                 %  and link is going down or flat
            x(i,:) = x(i-1,:)-[l_link 0];
         end

         if and(top == 0,x(i,1) <= -c2c/2)
                                 % if it is not in the top regime
                                 %  and the link is past the flat
                                 %  section this corresponds to
                                 %  section 4 of the chain.  p9
            xbuff = zeros(1,2);
            xbuff(1,:) = x(i-1,:) + [c2c/2 0];
            [x2,y2] = solve('l_link = sqrt((xbuff(1,1) -
x2)^2+(xbuff(1,2)-y2)^2)','r^2 = x2^2+y2^2');
            x(i,1) = min(eval(x2))-c2c/2;

            if through == 1
               buff = (eval(y2));
               x(i,2) = buff(1);
            else
               buff = (eval(y2));
               x(i,2) = buff(2);
               through = 1;
            end
            if x(i,2) >=0
               if thru == 1
                  x(i,1) = max(eval(x2))-c2c/2 ;
               else
                  x(i,1) = min(eval(x2))-c2c/2 ;
                  thru = 1;
               end

            end
         end
      end

      (x(i) - x(1))
      if abs(x(i) - x(1)) <= .0001
```

```
      done = 1;
   else
      r = r+(x(i) - x(1))/2/pi*1 % refine the radius at which
                                 %  the chain rides on the pulley
   end
end

X = x(1:n_links,:)/1000;         % output the position matrix for
                                 %  the chain link CGs (m)
r = r/1000  ;                    % pulley radius at which the
                                 %  chain rides (m)

if plotting == 1
   figure
   plot(X(:,1),X(:,2),'-')
   axis equal
   grid
else
   disp('plotting off')
end

%%%%%%%%%%%%%%%%%%%%%%%%%%%%%%%%%%%%%%%%%%%%%%%%%%%%%%%%%%%%%%%%%%%%%%%

disp('Link Direction and Velocity Initialization...')

for i=1:length(X)
   a = i-1;
   b = i;
   c = i+1;

   if i == 1
      a = n_links;            % index of m-1
      b = 1;                  % index of m
      c = 2;                  % index of m+1
   end
   if i == n_links
      a = n_links-1;          % index of m-1
      b = n_links;            % index of m
      c = 1;                  % index of m+1
   end

   dx = x(c,1)- x(a,1);
   dy = x(c,2) - x(a,2);
   theta(i) = atan2(dy,dx);

   theta_vect(i,1:2) = 1/sqrt(dx^2+dy^2)*[dx dy];
   speed = 100*2*pi/60*r;
end
theta(56) = -theta(56);



%initialize the Y vector for DOFs of the system
Y(1:length(X)) = X(:,1);   % link x position (m)
Y((length(X)+1):(2*length(X))) = X(:,2);
                           % link y position (m)
Y((2*length(X)+1):(3*length(X))) = theta-2*pi;
```

```
                                % link theta position (rad)
   Y((3*length(X)+1):(6*length(X))) = zeros(3*length(X),1);
                                % link xdot, ydot, thetadot (kg-
                                %  m/s,kg-m/s,kg-m^2-rad/s)
   Y(6*length(X)+1:6*length(X)+4) = [0 -0.1 0 -0.1];
                                % pulley [position mom.] for the
                                %  first and second pulleys
   Y = Y;                       % makes Y a column vector ready for
                                %  ode solver
   Y0 = Y';                     % makes Y0 a column vector ready
                                %  for ode solver
   %start_up

end

Z = zeros(n_links,1);
if r >= 1
   r = r/1000  ;                % pulley radius at which the chain
                                %  rides (m)
end
disp('Link Characteristics Initialization...')

l_link = 9.33/1000;             % GCI link length (mm)

a = -1.5371;

C_b = 100*[100 0 ; 0 100];      % Damping Matrix (Ns/m)
A_bc = [-5.5269 0]'*1e-3;
B_bc = [3.8032 0]'*1e-3;
A_b = [-3.7152 a]'*1e-3;
B_b = [5.6149 a]'*1e-3;

M = .031;                       % mass of one link, validated from
                                %  Chain_inertia_calc.xls, (kg)
I_link = 1.195E-03;             % inertia of one link, validated
                                % from Chain_inertia_calc.xls,
                                %  (kg-m^2)
r_pin = .30;                    % radius of the crowning on pin (m)
K_link = (1/contact_valid(M,1)+1/1.059e8)^(-1)*2/10;
K_link = K_link/20;


K_b = 2.0761e9*[1 0 ; 0 1]*1; % Compliance Matrix (N/m)
w_link = 0.030/2;               % width of the link (m)


disp('Pulley Characteristic Initialization...')

c2c = 167.99/1000;              % Nissan 2L CVT center to center
                                %  pulley distance (m)
center1 = [-c2c/2 0]';          % position of the center of the
                                %  primary pulley (m)
center2 = -center1;             % posiion of the center of the
                                %  secondary pulley (m)
pulley_beta = deg2rad(11);      % pulley sheave half angle (rad)
z0 = 0.0030
Z_out = zeros(n_links,1);
```

```
F_clamp = 10;                   % total compressive force from each
                                %  pulley (N)
w_p = [0 0 0]';                 % pulley angular velocity, negative is
                                %  CW (rad/sec)
mu_s = 0.12;                    % coefficient of static friction
mu_d = .09;                     % coefficient of dynamic friction
J_pulley = 0.028;               % rotational moment of inertia for the
                                %  pulley (kg-m^2)
step = 0;
%h = waitbar(0,'Tom this is your thesis talking.  Your ass is
mine!!!');
t_end = 1e-2
tspan = [0:t_end/500:t_end];%[0 t_end];%
size(Y0)
disp('Done - gci_init_v13f.m')

%%%%%%%%%%%%

disp('Running - gci_ode_v13f.m')
Y = Y0';
step = 0;
output_step = 1;
done = 0;
time = 0;
dh = 5e-6;
while ~done
   step = step+1  ;
   dYdt1 = gci_ode_v13f(time,Y,Y0);
   dYdt2 = gci_ode_v13f(time+dh/2, Y+dh/2*dYdt1, Y0);
   dYdt3 = gci_ode_v13f(time+dh/2, Y+dh/2*dYdt2, Y0);
   dYdt4 = gci_ode_v13f(time+dh, Y+dh*dYdt3, Y0);
   Y_next = Y + 1/6*(dYdt1 + 2*dYdt2 + 2*dYdt3 + dYdt4)*dh;
   Y_out(step,:) = Y';

   if step == 1
      time_prev = 0;
   else
      time_prev = time(step-1);
   end
   time(step) = time_prev+dh;

   if time(step) >= t_end
      done = 1;
   end
   Y = Y_next;
   time(length(time))
end

toc

toc
save chain_output21_30
end
sound((sin((5*[1:10000]))))
```

chain_ode_v13f.m

```
function dYdt = chain_ode_v13f(t,Y,Y0)
%This m-file determines the system of equations and outputs dY/dt.
%Thomas Bradley 7/8/01
global c2c l_link n_links A_b B_b r K_b C_b M center1 center2
global pulley_beta contact_flag force_comp w_p U C_mat A_mat
global A_e B_e h step contact_flag_out dYdt_pre t_end K_e C_e R
global F_clamp K_link w_link z0 F_t F_n e_v_contactt
global mu_s mu_d e_F_l e_t_l e_n_l r_pulley dist_c e_r_sigp e_n_p
global m_out e_v_contactn m  e_t_p U_out dYdt_1 Z
global I_link t_end_last J_pulley Z_out Y_test contact_flag2 cf_out
global pulley_i A_ec Z_last A_bc B_bc e_v_pullc
global e_v_contact_tangential

% define the System Dynamics Matrix A_mat
A_mat = sparse(zeros(6*n_links+4));
% define the Non-linearities Dynamics Matrix C-mat
C_mat = sparse(zeros(6*n_links+4));
U = sparse(zeros(6*n_links+4,1));
contact_flag = zeros(n_links,1);

qy_i = n_links;                     % index to get the y values in Y
qtheta_i = 2*n_links;               % index to get the theta values
in Y
px_i = 3*n_links;                   % index to get the x_dot values
                                    %  in Y, and the x_ddot solution
                                    %  row in A_mat
py_i = 4*n_links;                   % index to get the y_dot values
                                    %  in Y
ptheta_i = 5*n_links;               % index to get the theta_dot
                                    %  values in Y
pulley_i = 6*n_links;

%%%%%%%%%%%%%%%%%%%%%%%%%%%%%%%%%%%%%%%%%%%%%%%%%%%%%%%%%%%%%%%%%%%%%%%%%%%
U(pulley_i+2) = -100;          % Primary Pulley input torque (Nm)
U(pulley_i+4) = -100;          % Secondary Pulley output torque (Nm)
%%%%%%%%%%%%%%%%%%%%%%%%%%%%%%%%%%%%%%%%%%%%%%%%%%%%%%%%%%%%%%%%%%%%%%%%%%%

K_e = K_b(1,1);
C_e1 = C_b(1,1);                % this is the xy damping constant
C_e2 = C_b(1,1)/100;            % this is the damping constant for
                                %  theta
C_e3 = C_b(1,1)/10;             % this is the damping constant for
                                %  theta also

for m = 1:n_links;
   a = m-1;
   b = m;
   c = m+1;
   if m == 1
       a = n_links;             % index of m-1
       b = 1;                   % index of m
       c = 2;                   % index of m+1
   end
   if m == n_links
```

```
      a = n_links-1;          % index of m-1
      b = n_links;            % index of m
      c = 1;                  % index of m+1
   end

   ind = [2*m-1 2*m];
   R(ind,1:2) = [ cos(Y(qtheta_i+m)) -sin(Y(qtheta_i+m));
                  sin(Y(qtheta_i+m)) cos(Y(qtheta_i+m))];
                              % array of transformation matrices


%%%%%%%%%%%%%% This section is to determine the position of the
inter-link contact point on the A_b side of the link %%%%%%%%%%%%%%

   Rb = 0.0;
   t_i =  asin(sin(Y(qtheta_i+a))*cos(Y(qtheta_i+m)) -
sin(Y(qtheta_i+m))*cos(Y(qtheta_i+a)));   % t_i is the angle
position difference between
   tout(m) = t_i;
   x_t = -Rb*(sin(t_i) - (t_i)*cos(t_i));%-
Rb*SIN(G12)+Rb*G12*COS(G12)
   y_t = Rb*(cos(t_i) + (t_i)*sin(t_i))-
Rb;%Rb*COS(G12)+Rb*G12*SIN(G12)-Rb
   if t_i <= 0
      x_t = 0;
      y_t = 0;
   end

   A_e(m,1:2) = (R(ind,1:2)*(A_b+[x_t y_t]'))';


%%%%%%%%%%%%%% This section is to determine the position of the pin
%to sheave contact point on both sides of the link %%%%%%%%%%%%%%

   A_e_buff = R(ind,1:2)*A_bc;
   B_e_buff = R(ind,1:2)*B_bc;
   A_ec(m,1:2) = A_e_buff';
   B_ec(m,1:2) = B_e_buff';


%%%%%%%%%%%%%% This section is to determine the position of the
%inter-link contact point on the B_b side of the link %%%%%%%%%%%%%%

   ind = [2*c-1 2*c];
   R(ind,1:2) = [ cos(Y(qtheta_i+c)) -sin(Y(qtheta_i+c));
                  sin(Y(qtheta_i+c)) cos(Y(qtheta_i+c))];
                              % array of transformation matrices
   t_i_plus_1 = asin(sin(Y(qtheta_i+m))*cos(Y(qtheta_i+c)) -
sin(Y(qtheta_i+c))*cos(Y(qtheta_i+m)));
                              % t_i is the angle position difference
                              %  between the two links


   x_t = -Rb*(sin(t_i_plus_1) - (t_i_plus_1)*cos(t_i_plus_1));
```

```
            % equation of the involute
   y_t = Rb*(cos(t_i_plus_1) + (t_i_plus_1)*sin(t_i_plus_1))-Rb;
            % equation of the involute
   if t_i_plus_1 <= 0 %keeps the involute from going backwards
      x_t = 0;
      y_t = 0;
   end

   B_e(m,1:2) = (R([2*m-1 2*m],1:2)*(B_b + 0.5*Rb*t_i_plus_1^2))' ;
            % coord x-formation of B_b plus the involute arc length
end


for pulley = 1:2 % integrate to get pulley position from momentum
   A_mat(pulley_i+2*pulley-1,pulley_i+2*pulley) = 1/J_pulley;
end

for m = 1:n_links
   a = m-1;
   b = m;
   c = m+1;
   if m == 1
      a = n_links;            % index of m-1
      b = 1;                  % index of m
      c = 2;                  % index of m+1
   end
   if m == n_links
      a = n_links-1;          % index of m-1
      b = n_links;            % index of m
      c = 1;                  % index of m+1
   end
                % The 1st portion of A_mat corresponds to
                %  x_dot = A_mat x + B_mat u where x_dot = x_dot
   A_mat(m,px_i+m) = 1/M;
                % The next portion of A_mat corresponds to
                %  y_dot = A_mat x+B_mat u where y_dot = y_dot
   A_mat(qy_i+m,py_i+m) = 1/M;
                % The next portion of A_mat corresponds to
                %  theta_dot = A_mat x+B_mat u where
                %  theta_dot = theta_dot
   A_mat(qtheta_i+m,ptheta_i+m) = 1/I_link;
                % The next portion of A_mat corresponds to
                % x_ddot = A_mat x+B_mat u where x_ddot = sum F

   % assign the values to the A_mat that define px
   A_mat(px_i+m,a) = K_e;
   A_mat(px_i+m,b) = -2*K_e;
   A_mat(px_i+m,c) = K_e;

   C_mat(px_i+m,a) = K_e*B_e(a,1);
   C_mat(px_i+m,b) = -K_e*(B_e(b,1)+A_e(b,1));
   C_mat(px_i+m,c) = K_e*A_e(c,1);

   % assign the values to the A_mat that define py
   A_mat(py_i+m,qy_i+a) = K_e;
   A_mat(py_i+m,qy_i+b) = -2*K_e;
   A_mat(py_i+m,qy_i+c) = K_e;
```

```
   C_mat(py_i+m,qy_i+a) = K_e*B_e(a,2);
   C_mat(py_i+m,qy_i+b) = -K_e*(B_e(b,2)+A_e(b,2));
   C_mat(py_i+m,qy_i+c) = K_e*A_e(c,2);

   % assign the values to the A_mat that define ptheta

   A_mat(ptheta_i+m,a) = -K_e * A_e(b,2);
   A_mat(ptheta_i+m,b) = K_e * A_e(b,2) + K_e * B_e(b,2) ;
   A_mat(ptheta_i+m,c) = -K_e * B_e(b,2);

   C_mat(ptheta_i+m,a) = -K_e * A_e(b,2) * B_e(a,1);
   C_mat(ptheta_i+m,b) = 0;
   C_mat(ptheta_i+m,c) = -K_e * A_e(c,1) * B_e(b,2);

   A_mat(ptheta_i+m,qy_i+a) = K_e * A_e(b,1);
   A_mat(ptheta_i+m,qy_i+b) = -K_e * A_e(b,1) - K_e * B_e(b,1);
   A_mat(ptheta_i+m,qy_i+c) = K_e * B_e(b,1);

   C_mat(ptheta_i+m,qy_i+a) = K_e * B_e(a,2) * A_e(b,1);
   C_mat(ptheta_i+m,qy_i+b) = 0;
   C_mat(ptheta_i+m,qy_i+c) = K_e * B_e(b,1) * A_e(c,2);

   % assign the values to the A_mat that define px damping terms

   A_mat(px_i+m,px_i+a) = C_e1;
   A_mat(px_i+m,px_i+b) = -2*C_e1;
   A_mat(px_i+m,px_i+c) = C_e1;

   A_mat(px_i+m,ptheta_i+a) = C_e1 * B_e(a,2);
   A_mat(px_i+m,ptheta_i+b) = -C_e1 * (B_e(b,2) + A_e(b,2));
   A_mat(px_i+m,ptheta_i+c) = C_e1 * A_e(c,2);

   % assign the values to the A_mat that define py

   A_mat(py_i+m,py_i+a) = C_e1;
   A_mat(py_i+m,py_i+b) = -2*C_e1;
   A_mat(py_i+m,py_i+c) = C_e1;

   A_mat(py_i+m,ptheta_i+a) = C_e1 * B_e(a,1);
   A_mat(py_i+m,ptheta_i+b) = -C_e1 * (B_e(b,1) + A_e(b,1));
   A_mat(py_i+m,ptheta_i+c) = C_e1 * A_e(c,1);

   % assign the values to the A_mat that define the theta
   %  direction damping

   A_mat(ptheta_i+m,px_i+a) = -C_e2/M* A_e(b,2);
   A_mat(ptheta_i+m,px_i+b) = C_e2/M* A_e(b,2) + C_e2/M* B_e(b,2);
   A_mat(ptheta_i+m,px_i+c) = -C_e2/M* B_e(b,2);

   A_mat(ptheta_i+m,py_i+a) = C_e2/M* A_e(b,1);
   A_mat(ptheta_i+m,py_i+b) = -C_e2/M* A_e(b,1) - C_e2/M* B_e(b,1);
   A_mat(ptheta_i+m,py_i+c) = C_e2/M* B_e(b,1);

   A_mat(ptheta_i+m,ptheta_i+a) = C_e3/I_link* B_e(a,1)*A_e(b,1) +
C_e3/I_link* B_e(a,2)*A_e(b,2);
```

```
   A_mat(ptheta_i+m,ptheta_i+b) = -C_e3/I_link* A_e(b,1)*A_e(b,1) -
C_e3/I_link* B_e(b,1)*B_e(b,1) - C_e3/I_link* A_e(b,2)*A_e(b,2) -
C_e3/I_link * B_e(b,2)*B_e(b,2) ;
   A_mat(ptheta_i+m,ptheta_i+c) = C_e3/I_link* A_e(c,1)*B_e(b,1) +
C_e3/I_link* A_e(c,2)*B_e(b,2);

end
dYdt_1 = A_mat*Y+C_mat*ones(size(U));
%%%%%%%%%%%%%%%%%%%%%%%%%%%%%% Contact Mechanics %%%%%%%%%%%%%%%%%%%%%%
theta_l = -pulley_beta;
% This makes the contact always happen at the the center of the pin
%  This does not capture the roundness of the pin
Y_test = Y;

for m = 1:n_links
   if Y(m) >= 0
      theta_p = atan2(-center2(2,1) + (Y(qy_i+m) + A_ec(m,2)),-
center2(1,1) + (Y(m) + A_ec(m,1))) ;
      e_r_p = [center2(1,1) center2(2,1) 0]';
                        % position vector of the pulley center (m)
      cf = 2;
   else
      theta_p = atan2((-center1(2,1) + (Y(qy_i+m) + A_ec(m,2))),(-
center1(1,1) + (Y(m) + A_ec(m,1)))) ;
      e_r_p = [center1(1,1) center1(2,1) 0]';
                        % position vector of the pulley center (m)
      cf = 1;
   end

   r_pulley = sqrt((-e_r_p(2,1) + (Y(qy_i+m) + A_ec(m,2)))^2 + (-
e_r_p(1,1) + (Y(m) + A_ec(m,1)))^2);

   e_r_sigp = [cos(theta_p) sin(theta_p) tan(pulley_beta)]'*r_pulley
+ [0 0 z0]' ;           % position vector of the contour of the
                        %  pulley in earth coords from the center of
                        %  the pulley
   e_n_p3 = [cos(theta_p)*sin(pulley_beta)
sin(theta_p)*sin(pulley_beta) -cos(pulley_beta)]';
                        % pulley normal vector in earth coords (1)
   e_t_p2 = [-sin(theta_p) cos(theta_p) 0]';
                        % pulley tangent vector in earth coords (2)
   e_t_p1 = cross(e_t_p2,e_n_p3);
                        % pulley tangent vector in earth coords
                        %  facing up at theta = 0 (3)
   e_r_sigl = [ 0 0 (w_link)]' + [A_ec(m,1) A_ec(m,2) 0]';
                        % position vector of the contour of the pin
                        %  in earth coords
   e_r_dist = e_r_sigl + [Y(m) Y(qy_i+m) 0]' - e_r_sigp - e_r_p;
                        % distance vector between the pulley contact
                        %  and the pin from the pulley to the pin
   if norm(e_r_dist) == 0
      contact_bool = 1;
   else
      contact_bool = ((e_r_dist/norm(e_r_dist))'*e_n_p3 <= 0);
   end
```

```
   if contact_bool == 1
      e_v_pullc=cross(1/J_pulley*[0 0 Y(pulley_i+2*cf)]',e_r_sigp) ;
      contact_flag(m) = cf;
      e_v_linkc = 1/M*[Y(px_i+m) Y(py_i+m) 0]' + cross(1/I_link*[0 0
Y(ptheta_i+m)]',e_r_sigl);
                        % velocity in earth coords of the link
                        %  contact point.  (v_link = v_cg + w x
                        %  r_contact_point)
      e_v_contact = e_v_pullc - e_v_linkc;
                        % velocity of the pulley in the earth coords
                        %  of the pulley from the pin
      e_v_contact1 = e_v_contact'*e_t_p1;
      e_v_contact2 = e_v_contact'*e_t_p2;
      e_v_contact3 = e_v_contact'*e_n_p3;
                        % mag of relative velocity in each direction

      e_v_contact_tangential = sqrt(e_v_contact1^2 +
e_v_contact2^2);        % mag of relative velocity in the plane of
                        %  the pin contact
      Z(m) = (r_pulley*tan(pulley_beta)+z0-w_link);
      if Z(m) >= 0
         Z(m) = 0;
      end

      e_F_l = [dYdt_1(px_i+m) dYdt_1(py_i+m) (+K_link*abs(Z(m)))]'+
e_n_p3*K_link*abs(Z(m))^(1)/cos(pulley_beta);
                        % sum of the  external force on the link

      F_n3 = +K_link*abs(Z(m))^(1)/cos(pulley_beta);
      F_t2 = e_F_l'*e_t_p2;
      F_t1 = e_F_l'*e_t_p1;

      will_it_stick = 3;%<--------------------change this friction
      if will_it_stick == 0
         mu = 0.15*(1-exp(-e_v_contact_tangential/1)) ;
         F_t = mu*F_n3*(e_v_contact2*e_t_p2 +
e_v_contact1*e_t_p1)/e_v_contact_tangential;
         F_contact =   F_n3 * e_n_p3 + F_t;
         U(px_i+m,1) = -F_contact(1,1);
         U(py_i+m,1) = F_contact(2,1);
         U(ptheta_i+m,1) = -F_contact(1,1)*A_ec(m,2) +
F_contact(2,1)*A_ec(m,1);

      elseif will_it_stick == 2     %Leine et al friction
         epsilon = 1e10;   %friction steepness factor, Leine et. al.
         mu = 0.15*2/pi*atan(abs(e_v_contact_tangential)*epsilon)
/(1+3*abs(e_v_contact_tangential));
         if and(mu <= 0.06, abs(e_v_contact_tangential) >= 0.1)
            mu = 0.06;
         end
         F_t = (mu*F_n3)*(e_v_contact2*e_t_p2 +
e_v_contact1*e_t_p1)/sqrt(e_v_contact2^2 + e_v_contact1^2);
                        % Friction force opposite in direction of
                        %  the movement of the pulley relative to
                        %  the pin
         F_contact = F_n3 * e_n_p3 + F_t;
```

```
         U(px_i+m,1) = F_contact(1,1);
         U(py_i+m,1) = F_contact(2,1);

      else % Karnopp/Leine Friction Model
         mu =  0.2;
         if abs(e_v_contact_tangential) >= .1;     % slip
            F_t = mu*F_n3*(e_v_contact2*e_t_p2 +
e_v_contact1*e_t_p1)/sqrt(e_v_contact2^2 + e_v_contact1^2);
            F_contact =   F_n3 * e_n_p3 + F_t;
            U(px_i+m,1) = F_contact(1,1);
            U(py_i+m,1) = F_contact(2,1);

         elseif(sqrt((F_t2^2+F_t1^2)) > mu*F_n3*1.05)
                        % stick to slip transition
            F_t = (sqrt((F_t2^2+F_t1^2)) - mu*F_n3) *
(e_t_p2*sign(F_t2) + e_t_p1*sign(F_t1))/sqrt(2);
                        % mag(external force) - mag(friction)
            F_contact =  F_t + F_n3 * e_n_p3;
            U(px_i+m,1) = F_contact(1,1);
            U(py_i+m,1) = F_contact(2,1);
            %U(ptheta_i+m,1) = F_contact(2,1)*A_ec(m,1) -
F_contact(1,1)*A_ec(m,2);

         else                    % stick
            F_t = e_v_contact_tangential*sqrt(1000/M)
*(e_v_contact2*e_t_p2 + e_v_contact1*e_t_p1)/e_v_contact_tangential;
                        % mag * (-)direction of motion
            F_contact =   F_n3 * e_n_p3 + F_t;
                        % this is the 3-D vector of contact forces
                        %  at the point of contact
            U(px_i+m,1) =  F_contact(1,1);
            U(py_i+m,1) =  F_contact(2,1);
            %U(ptheta_i+m,1) = F_contact(2,1)*A_ec(m,1) -
F_contact(1,1)*A_ec(m,2);

        end
      end

      U(pulley_i+2*cf) = U(pulley_i+2*cf) - F_t'*e_t_p2*r_pulley;
                        % Pulley reaction torque (Nm)
   else
      F_contact = [0 0 0]'*1e3;
      Z(m) = 0;%
   end

end

dYdt = A_mat*Y+C_mat*ones(size(U))+U;
%return to gci_init program;
```

APPENDIX 3 – Linear Elastic Link Compliance

Calculation: MATLAB M-file

link_comp.m

```
clear
close all

%~~~~~~~~~~~~~~~~~~~~~~~~~~~~~~~~~~~~~~~~~~~~~~~~~~~~~~~~~~~~~~~~~~~~~~~~~~~~
~~~~~%
% PIN BENDING COMPLIANCE
%~~~~~~~~~~~~~~~~~~~~~~~~~~~~~~~~~~~~~~~~~~~~~~~~~~~~~~~~~~~~~~~~~~~~~~~~~~~~
~~~~~%

E = 2.068427e+011;
B = .003;
A = .010;
I = pi*B*A^3/4;
L = 30e-3;

A_1 = [0:8]*3*.00084 + 0.00492;
A_2 = [-10 -8 -4 -2 2 4 8 10]*.00084 + .015;
A_tot = [A_1 A_2];

for load = 1:10
   W = 35e3/10 * load / length(A_1);

   for j = 1:length(A_tot)
      x = [0:.0001:.030]';
      a = A_tot(j);

      if j > length(A_1)
         W = -35e3/10 * load / length(A_2);
      end

      for i = 1:length(x)

         if x(i) >= a
            F_v(i) = W * (x(i)-a)^3/(6*E*I);
            F_theta(i) = -W * (x(i)-a)^2/(2*E*I);
         else
            F_v(i) = 0;
            F_theta(i) = 0;
         end

         M_0 = 6*E*I/(L^2)*W * (L-a)^3/(6*E*I) + 2*E*I/L*(-W*(L-
a)^2/(2*E*I));
         V_0 = -12*E*I/L^3*W * (L-a)^3/(6*E*I) - 6*E*I/L^2*(-W*(L-
a)^2/(2*E*I));

         y(i,j) = - M_0*x(i)^2/(2*E*I) - V_0*x(i)^3/(3*2*E*I) +
F_v(i);
```

```
      end
      hold on
      plot(x,y(:,j))

   end

   figure
   plot(x,sum(y,2))
   y_output = interp1(x,sum(y,2),A_tot);

   delta(load) = mean(y_output(1:length(A_1))) -
mean(y_output(10:length(y_output)));
end

load = [1:10];
W = 35e3/10 * load / length(A_1);
plot(W,delta)



%~~~~~~~~~~~~~~~~~~~~~~~~~~~~~~~~~~~~~~~~~~~~~~~~~~~~~~~~~~~~~~~~~~~~~~~~~~~~
~~~~~%
% HERTZ LINE CONTACT COMPLIANCE
%~~~~~~~~~~~~~~~~~~~~~~~~~~~~~~~~~~~~~~~~~~~~~~~~~~~~~~~~~~~~~~~~~~~~~~~~~~~~
~~~~~%

R = .040;
a = sqrt(4*W*R/pi/E);
delta = W.*(1-0.3^2)/pi/E .* (2*log(4*R./a)-1);
plot(W,delta, 'r')

%~~~~~~~~~~~~~~~~~~~~~~~~~~~~~~~~~~~~~~~~~~~~~~~~~~~~~~~~~~~~~~~~~~~~~~~~~~~~
~~~~~%
% LINK ELASTIC ELONGATION COMPLIANCE
%~~~~~~~~~~~~~~~~~~~~~~~~~~~~~~~~~~~~~~~~~~~~~~~~~~~~~~~~~~~~~~~~~~~~~~~~~~~~
~~~~~%

delta = W*9.16e-3/E/(.00084*.01366)/8;

plot(W,delta, 'k')
```